# Search for $1^{-+}$ charmoniumlike hybrid via $e^+e^- \to \gamma\eta^{(\prime)}\eta_c$ at center-of-mass energies between 4.258 and 4.681 GeV

M. Ablikim *et al.*[*]
(BESIII Collaboration)

(Received 20 April 2025; accepted 22 May 2025; published 20 June 2025)

Using $e^+e^-$ collision data corresponding to an integrated luminosity of 10.6 $\mathrm{fb}^{-1}$ collected at center-of-mass energies between 4.258 and 4.681 GeV with the BESIII detector at the BEPCII collider, we search for the $1^{-+}$ charmoniumlike hybrid via $e^+e^- \to \gamma\eta\eta_c$ and $e^+e^- \to \gamma\eta'\eta_c$ decays for the first time. No significant signal is observed, and the upper limits on the Born cross sections for both processes are set at the 90% confidence level.

DOI: 10.1103/2rq2-nr4m

## I. INTRODUCTION

Quantum chromodynamics (QCD) allows the existence of exotic hadron states beyond the quark model, such as glueballs, hybrids, multiquark states, and hadronic molecules. The search for these QCD exotic states is crucial for quantitatively testing the theory of strong interactions in nonperturbative regions and for understanding confinement. However, it is difficult to distinguish the exotic hadron states from the conventional mesons. Hadrons with exotic $J^{PC}$ quantum numbers, such as $0^{--}$, $\mathrm{even}^{+-}$, and $\mathrm{odd}^{-+}$, cannot arise from ordinary $q\bar{q}$ states. Searching for such hadrons offers one of the most direct and unambiguous ways to establish the existence of exotic hadron states.

Lattice QCD predicts the existence of a series of light hybrid multiplets ($J^{PC} = 0^{-+}, 1^{--}, 1^{-+}$, and $2^{-+}$), with the exotic $1^{-+}$ nonet being the lightest [1]. Similar to the case of the hybrid multiplets composed of light quarks ($n\bar{n}g$), $c\bar{c}$ can also form analogous hybrid multiplets ($c\bar{c}g$) [2,3]. In the charmonium sector, four confirmed states, $\psi(4230)$, $\psi(4360)$, $\psi(4390)$, and $\psi(4660)$, fall within the mass range expected for $1^{-+}$ hybrid charmonia [4–7].

Three light isovector states, the $\pi_1(1400)$, $\pi_1(1600)$, and $\pi_1(2015)$ [8–11], have been experimentally identified as exotic hadrons exhibiting the quantum numbers $J^{PC} = 1^{-+}$. Recently, BESIII collaboration performed a partial wave analysis of the $J/\psi \to \gamma\eta\eta'$ decay process, and reported the first observation of a nonconventional state $\eta_1(1855)$ with the exotic quantum numbers $I^G J^{PC} = 0^+1^{-+}$ [12,13]. However, no state with manifestly exotic $J^{PC}$ has been observed in the charmonium region. Analogous to the $\eta_1(1855) \to \eta\eta'$ process, a possible $\eta_{c1}$ state could decay into $\eta^{(\prime)}\eta_c$ final states. Additionally, some theoretical predictions suggest that the $1^{-+}$ charmoniumlike hybrid state might also decay to $\eta^{(\prime)}\eta_c$ final states [14,15].

In this paper, we report a study of $e^+e^- \to \gamma\eta^{(\prime)}\eta_c$ to search for the $1^{-+}$ charmoniumlike hybrid state based on data samples collected with the BESIII detector at center-of-mass (c.m.) energies between 4.258 and 4.681 GeV, listed in Table I. The integrated luminosities of these data samples are determined by analyzing large-angle Bhabha scattering events with an uncertainty of 1.0%, and the c.m. energies are measured using the dimuon process [16,17].

## II. BESIII DETECTOR AND MONTE CARLO SIMULATION

The BESIII detector [18] records symmetric $e^+e^-$ collisions provided by the BEPCII storage ring [19] in the c.m. energy range from 1.84 to 4.95 GeV, with a peak luminosity of $1.1 \times 10^{33}\ \mathrm{cm}^{-2}\,\mathrm{s}^{-1}$ achieved at $\sqrt{s} = 3.773$ GeV. BESIII has collected large data samples in this energy region [20,21]. The cylindrical core of the BESIII detector covers 93% of the full solid angle and consists of a helium-based multilayer drift chamber (MDC), a time-of-flight system (TOF), and a CsI(Tl) electromagnetic calorimeter (EMC), which are all enclosed in a superconducting solenoidal magnet providing a 1.0 T magnetic field. The solenoid is supported by an octagonal flux-return yoke with resistive plate counter muon identification modules interleaved with steel. The charged-particle momentum resolution at 1 GeV/$c$ is 0.5%, and the $\mathrm{d}E/\mathrm{d}x$ resolution is 6% for electrons from Bhabha scattering. The EMC measures photon energies with a resolution of 2.5% (5%) at 1 GeV in the barrel (end cap) region. The time resolution of the plastic scintillator TOF in

[*]Full author list given at the end of the article.

TABLE I. Datasets and results of the upper limits on Born cross sections of $e^+e^- \to \gamma\eta^{(\prime)}\eta_c$: the integrated luminosities $\mathcal{L}$, the upper limits of observed signal yields $N_{\rm UL}^{\rm obs}$, the ISR correction $(1+\delta)$, the vacuum polarization correction factor $\frac{1}{|1-\Pi|^2}$, the sum of the products of the branching fraction and efficiency $\sum \mathcal{B}_i\epsilon_i$, the upper limits of Born cross sections $\sigma_{\rm UL}^{\rm Born}$(pb), and the statistical significance $\mathcal{S}$.

| | | $e^+e^- \to \gamma\eta\eta_c$ | | | | | | $e^+e^- \to \gamma\eta'\eta_c$ | | | | | |
|---|---|---|---|---|---|---|---|---|---|---|---|---|---|
| $\sqrt{s}$ (GeV) | $\mathcal{L}$(pb$^{-1}$) | $1+\delta$ | $\frac{1}{\vert 1-\Pi\vert^2}$ | $N_{\rm UL}^{\rm obs}$ | $\sum_i(\mathcal{B}_i\epsilon_i)(\%)$ | $\sigma_{\rm UL}^{\rm Born}$ (pb) | $\mathcal{S}(\sigma)$ | $1+\delta$ | $\frac{1}{\vert 1-\Pi\vert^2}$ | $N_{\rm UL}^{\rm obs}$ | $\sum_i(\mathcal{B}_i\epsilon_i)(\%)$ | $\sigma_{\rm UL}^{\rm Born}$ (pb) | $\mathcal{S}(\sigma)$ |
| 4.258 | 828.4 | 0.86 | 1.05 | 76.8 | 0.38 | 27.3 | 0.1 | 0.85 | 1.05 | 65.8 | 0.17 | 51.2 | 2.8 |
| 4.267 | 531.1 | 0.86 | 1.05 | 62.3 | 0.37 | 35.3 | 0.1 | 0.85 | 1.05 | 45.6 | 0.17 | 56.4 | 1.5 |
| 4.278 | 175.7 | 0.86 | 1.05 | 28.2 | 0.36 | 49.1 | 2.2 | 0.85 | 1.05 | 28.3 | 0.16 | 110.1 | 1.9 |
| 4.288 | 502.4 | 0.86 | 1.05 | 30.6 | 0.37 | 18.5 | 0.6 | 0.86 | 1.05 | 33.4 | 0.17 | 44.5 | 2.5 |
| 4.308 | 45.1 | 0.85 | 1.05 | 36.2 | 0.37 | 240.8 | 2.5 | 0.84 | 1.05 | 12.6 | 0.18 | 178.9 | 1.7 |
| 4.312 | 501.2 | 0.85 | 1.05 | 48.5 | 0.36 | 29.6 | 1.9 | 0.87 | 1.05 | 43.7 | 0.17 | 56.5 | 2.8 |
| 4.337 | 505.0 | 0.85 | 1.05 | 61.3 | 0.37 | 26.8 | 0.9 | 0.87 | 1.05 | 44.2 | 0.17 | 55.2 | 2.8 |
| 4.358 | 543.9 | 0.85 | 1.05 | 38.8 | 0.38 | 21.1 | 0.6 | 0.84 | 1.05 | 65.0 | 0.18 | 75.5 | 2.4 |
| 4.377 | 522.7 | 0.84 | 1.05 | 48.4 | 0.37 | 28.2 | 1.5 | 0.86 | 1.05 | 40.2 | 0.18 | 48.5 | 1.0 |
| 4.387 | 55.6 | 0.84 | 1.05 | 13.7 | 0.38 | 73.6 | 2.5 | 0.84 | 1.05 | 14.6 | 0.18 | 165.2 | 1.3 |
| 4.396 | 507.8 | 0.84 | 1.05 | 35.1 | 0.37 | 21.1 | 2.5 | 0.86 | 1.05 | 34.1 | 0.18 | 42.7 | 0.6 |
| 4.416 | 1043.9 | 0.83 | 1.05 | 45.2 | 0.37 | 13.2 | 0.1 | 0.84 | 1.05 | 70.9 | 0.18 | 41.9 | 2.3 |
| 4.436 | 569.9 | 0.83 | 1.05 | 91.3 | 0.38 | 49.3 | 1.1 | 0.85 | 1.05 | 32.4 | 0.18 | 35.3 | 1.1 |
| 4.467 | 111.1 | 0.82 | 1.05 | 27.5 | 0.38 | 77.1 | 0.8 | 0.82 | 1.05 | 13.7 | 0.18 | 79.3 | 0.9 |
| 4.527 | 112.1 | 0.81 | 1.05 | 60.0 | 0.38 | 38.9 | 2.0 | 0.81 | 1.05 | 16.2 | 0.19 | 90.0 | 1.0 |
| 4.574 | 48.9 | 0.79 | 1.05 | 24.1 | 0.38 | 179.7 | 1.5 | 0.79 | 1.05 | 12.6 | 0.20 | 158.7 | 0.4 |
| 4.600 | 586.9 | 0.78 | 1.05 | 60.6 | 0.38 | 32.7 | 2.4 | 0.78 | 1.05 | 17.4 | 0.20 | 18.4 | 0.9 |
| 4.611 | 103.65 | 0.77 | 1.05 | 24.0 | 0.38 | 78.5 | 0.7 | 0.77 | 1.05 | 12.9 | 0.20 | 78.3 | 0.1 |
| 4.628 | 521.53 | 0.77 | 1.05 | 77.6 | 0.38 | 48.8 | 1.3 | 0.77 | 1.05 | 27.4 | 0.20 | 33.7 | 1.2 |
| 4.641 | 551.65 | 0.76 | 1.05 | 28.7 | 0.38 | 17.3 | 2.2 | 0.76 | 1.05 | 25.1 | 0.20 | 28.8 | 0.2 |
| 4.661 | 529.43 | 0.75 | 1.05 | 55.9 | 0.38 | 35.4 | 1.2 | 0.75 | 1.05 | 29.0 | 0.20 | 34.4 | 1.5 |
| 4.681 | 1667.39 | 0.75 | 1.05 | 71.8 | 0.38 | 14.5 | 1.4 | 0.78 | 1.05 | 46.1 | 0.20 | 16.5 | 0.4 |

the barrel region is 68 ps, while that in the end cap region is 110 ps. In 2015, the end cap TOF system was upgraded with multigap resistive plate chamber technology, improving the time resolution to 60 ps, which benefits approximately 68% of the data used in this analysis [22–24].

Monte Carlo (MC) simulated data samples produced with a GEANT4-based software package [25], which includes the geometric description of the BESIII detector and the detector response, are used to determine detection efficiencies and to estimate backgrounds. The simulation models the beam energy spread and initial state radiation (ISR) in the $e^+e^-$ annihilations with the generator KKMC [26,27]. In this analysis, 100,000 MC events are generated for each decay mode of $\eta_c$ at each c.m. energy with KKMC and EVTGEN [28,29]. The inclusive MC samples include the production of open-charm processes, the ISR production of vector charmonium(like) states, and the continuum processes incorporated in KKMC. All particle decays are modeled with EVTGEN using branching fractions taken from the Particle Data Group (PDG) [30], when available, or otherwise estimated with LUNDCHARM [31]. Final-state radiation from charged final-state particles is incorporated using the PHOTOS package [32].

## III. EVENT SELECTION AND STUDY OF BACKGROUND

To select candidate events for $e^+e^- \to \gamma\eta^{(\prime)}\eta_c$, the $\eta'$ is reconstructed through the final states of $\eta\pi^+\pi^-$, the $\eta_c$ is reconstructed through 16 hadronic final states: $p\bar{p}$, $2(\pi^+\pi^-)$, $2(K^+K^-)$, $K^+K^-\pi^+\pi^-$, $p\bar{p}\pi^+\pi^-$, $3(\pi^+\pi^-)$, $K^+K^-2(\pi^+\pi^-)$, $K^+K^-\pi^0$, $p\bar{p}\pi^0$, $K_S^0K^\pm\pi^\mp$, $K_S^0K^\pm\pi^\mp\pi^\pm\pi^\mp$, $\pi^+\pi^-\eta$, $K^+K^-\eta$, $2(\pi^+\pi^-)\eta$, $\pi^+\pi^-\pi^0\pi^0$, and $2(\pi^+\pi^-)\pi^0\pi^0$, in which $K_S^0$ is reconstructed from its $\pi^+\pi^-$ decay, $\pi^0$ and $\eta$ from their $\gamma\gamma$ final state.

Charged tracks detected in the MDC must be within a polar angle ($\theta$) range of $|\cos\theta| < 0.93$, where $\theta$ is defined with respect to the $z$-axis, the symmetry axis of the MDC. For charged tracks not originating from $K_S^0$ decays, the distance of closest approach to the interaction point (IP) must be less than 10 cm along the $z$-axis, $|V_z|$, and less than 1 cm in the transverse plane, $|V_{xy}|$. By combining the energy deposit $\mathrm{d}E/\mathrm{d}x$ and the TOF information, the $\chi^2_{\rm PID}(i)$ (where $i = K$, $\pi$, or $p$) is calculated for each charged track under different hadron hypotheses. Both PID and kinematic fit information are used to determine the particle type of each charged track.

Photon candidates are identified using isolated showers in the EMC. The deposited energy of each shower must exceed 25 MeV in the barrel region ($|\cos\theta| < 0.80$) and 50 MeV in the end cap region ($0.86 < |\cos\theta| < 0.92$). To exclude showers that originate from charged tracks, the angle between the EMC shower position and the closest charged track at the EMC must exceed 10 degrees, as measured from the IP. To suppress electronic noise and unrelated showers, the difference between the EMC time and the event start time must be within the range [0,700] ns.

Each $K_S^0$ candidate is reconstructed from two oppositely charged tracks satisfying $|V_z| < 20$ cm. The two charged tracks are assigned as $\pi^+\pi^-$ without imposing additional PID criteria. They are constrained to originate from a common vertex and are required to have an invariant mass within $|M_{\pi^+\pi^-} - m_{K_S^0}| < 20\ \mathrm{MeV}/c^2$, where $m_{K_S^0}$ is the $K_S^0$ nominal mass [30]. The decay length of the $K_S^0$ candidate is required to be greater than twice the vertex resolution away from the IP. The $\pi^0(\eta)$ candidates are selected with the invariant mass of $\gamma\gamma$ pair satisfying $|M_{\gamma\gamma} - m_{\pi^0(\eta)}| < 15\ \mathrm{MeV}/c^2$, where $m_{\pi^0(\eta)}$ is the nominal mass of $\pi^0(\eta)$ [30]. To improve the energy resolution, a one-constraint (1C) kinematic fit is performed with a constraint on the $\pi^0(\eta)$ mass.

After the above selections, four-constraint (4C) kinematic fits are performed for each event, imposing overall energy-momentum conservation with the $3\gamma(\pi^+\pi^-)+$ hadrons hypothesis, where hadrons represents the corresponding final states of the $\eta_c$ decay modes. The chi-square values of the 4C kinematic fit $\chi^2_{4C(3\gamma+\mathrm{hadrons})}$ and $\chi^2_{4C(3\gamma\pi^+\pi^-+\mathrm{hadrons})}$ are required to be less than 20 and 30, respectively, to suppress background events with different final states. For each $\eta_c$ decay mode, if there are multiple combinations satisfying the above criteria, only the one with the minimum total chi-square $\chi^2_{\mathrm{tot}} = \chi^2_{4C(3\gamma(\pi^+\pi^-)+\mathrm{hadrons})} + \chi^2_{\mathrm{PID}} + \chi^2_{1C} + \chi^2_{\mathrm{vertex}}$ is retained, where $\chi^2_{\mathrm{PID}}$ is the sum of the $\chi^2_{\mathrm{PID}}(i)$ for each charged track in the event, $\chi^2_{1C}$ is from the 1C kinematic fit for the $\pi^0(\eta)$ mass, and $\chi^2_{\mathrm{vertex}}$ is the $\chi^2$ of the $K_S^0$ secondary vertex fit. If there is no $\pi^0/\eta(K_S^0)$ in an event, the corresponding $\chi^2_{1C}(\chi^2_{\mathrm{vertex}})$ is set to zero.

For the $e^+e^- \to \gamma\eta\eta_c$ process, 4C kinematic fits are performed by constraining energy-momentum conservation

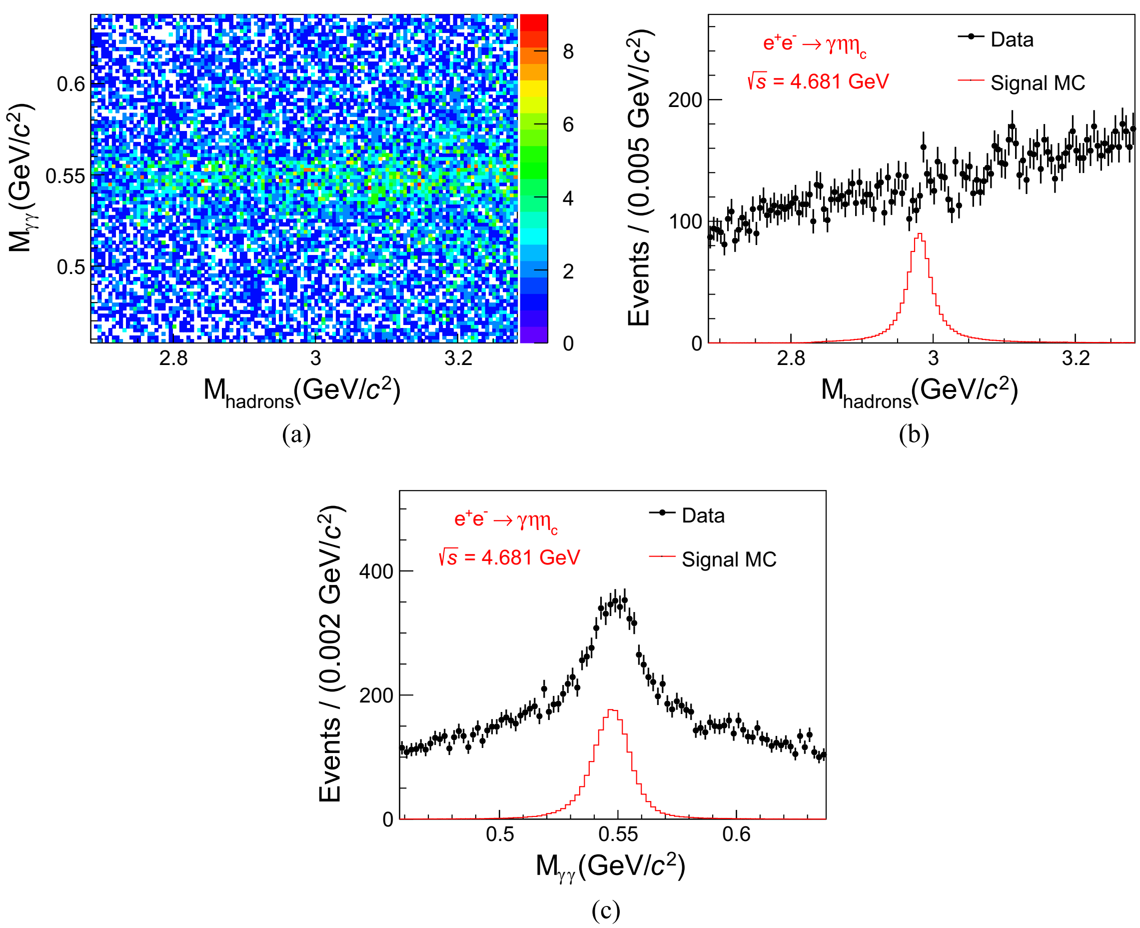


FIG. 1. The distributions of (a) $M_{\gamma\gamma}$ versus $M_{\mathrm{hadrons}}$, (b) $M_{\mathrm{hadrons}}$, and (c) $M_{\gamma\gamma}$ at $\sqrt{s} = 4.681$ GeV. For (b) and (c), the dots with error bars are data, and the red histograms represent the signal MC.

under the hypotheses $e^+e^- \to 2\gamma + \text{hadrons}$ and $e^+e^- \to 4\gamma + \text{hadrons}$, to suppress the backgrounds from processes with two or four photons in the final state. The $\chi^2_{4C(3\gamma+\text{hadrons})}$ is required to be less than all possible $\chi^2_{4C(2\gamma+\text{hadrons})}$ and $\chi^2_{4C(4\gamma+\text{hadrons})}$. In case of multiple $\eta_c$ candidates in an event, the one with the invariant mass closest to the $\eta_c$ nominal mass is selected to reconstruct the $\eta_c$ meson. Finally, the remaining $\eta$ candidate is chosen to reconstruct the $\eta$ meson from the $e^+e^-$ collision.

For the $e^+e^- \to \gamma\eta'\eta_c$ process, the $\eta_c$ and $\eta'$ candidates are formed from hadrons and $\eta\pi^+\pi^-$ combinations, respectively, with the least $\frac{(M_{\text{hadrons}}-m_{\eta_c})^2}{\sigma^2_{m_{\eta_c}}} + \frac{(M_{\eta\pi^+\pi^-}-m_{\eta'})^2}{\sigma^2_{m_{\eta'}}}$. Here, $m_{\eta_c}$ and $m_{\eta'}$ are the nominal masses of $\eta_c$ and $\eta'$, respectively [30], $M_{\text{hadrons}}$ is the invariant mass of the 16 different decay modes of $\eta_c$ mentioned above, $M_{\eta\pi^+\pi^-}$ is the invariant mass of $\eta\pi^+\pi^-$, and $\sigma_{m_{\eta'}}$ and $\sigma_{m_{\eta_c}}$ are the visible widths, determined by fitting the individual distributions with a Gaussian function and a Breit-Wigner function, respectively.

After applying the reconstructed selection criteria to all data samples, the two-dimensional distributions of $M_{\gamma\gamma}$ versus $M_{\text{hadrons}}$ and $M_{\eta\pi^+\pi^-}$ versus $M_{\text{hadrons}}$ in data and MC simulation at $\sqrt{s} = 4.681$ GeV are shown in Figs. 1(a) and 2(a), where $M_{\gamma\gamma(\eta\pi^+\pi^-)}$ is the invariant mass of the reconstructed $\eta^{(\prime)}$ from $e^+e^-$ collision. No significant $e^+e^- \to \gamma\eta^{(\prime)}\eta_c$ signals are observed in the projections of $M_{\gamma\gamma(\eta\pi^+\pi^-)}$ versus $M_{\text{hadrons}}$. The distributions of $M_{\text{hadrons}}$ and $M_{\gamma\gamma(\eta\pi^+\pi^-)}$ at $\sqrt{s} = 4.681$ GeV are shown in Figs. 1(b), 1(c), 2(b), and 2(c). Additionally, the distribution of $M_{\gamma\gamma}$ used for the reconstruction of the $\eta'$ is shown in Fig. 2(d).

Since the luminosity of data samples at $\sqrt{s} = 4.681$ GeV is the largest, we use the inclusive MC sample at this energy point, with the luminosity 40 times larger than the data to study the background components. After applying the mentioned selection criteria to the inclusive MC sample, no significant peaking backgrounds containing both $\eta_c$ and $\eta^{(\prime)}$ simultaneously are observed. However, for the $e^+e^- \to \gamma\eta\eta_c$ process, there are some background

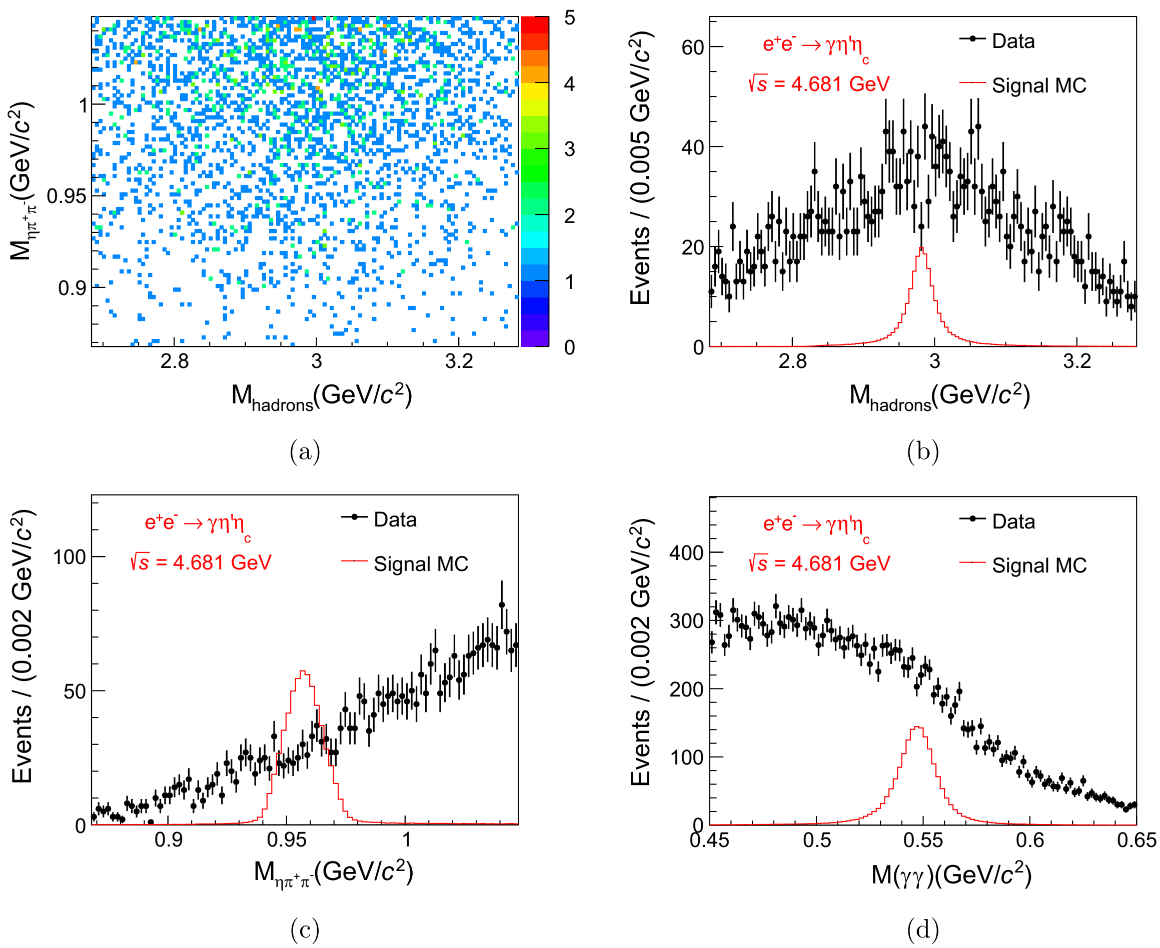


FIG. 2. The distributions of (a) $M_{\eta\pi^+\pi^-}$ versus $M_{\text{hadrons}}$, (b) $M_{\text{hadrons}}$, (c) $M_{\eta\pi^+\pi^-}$, and (d) $M_{\gamma\gamma}$ at $\sqrt{s} = 4.681$ GeV. For (b), (c), and (d), the dots with error bars are data, and the red histograms represent the signal MC.

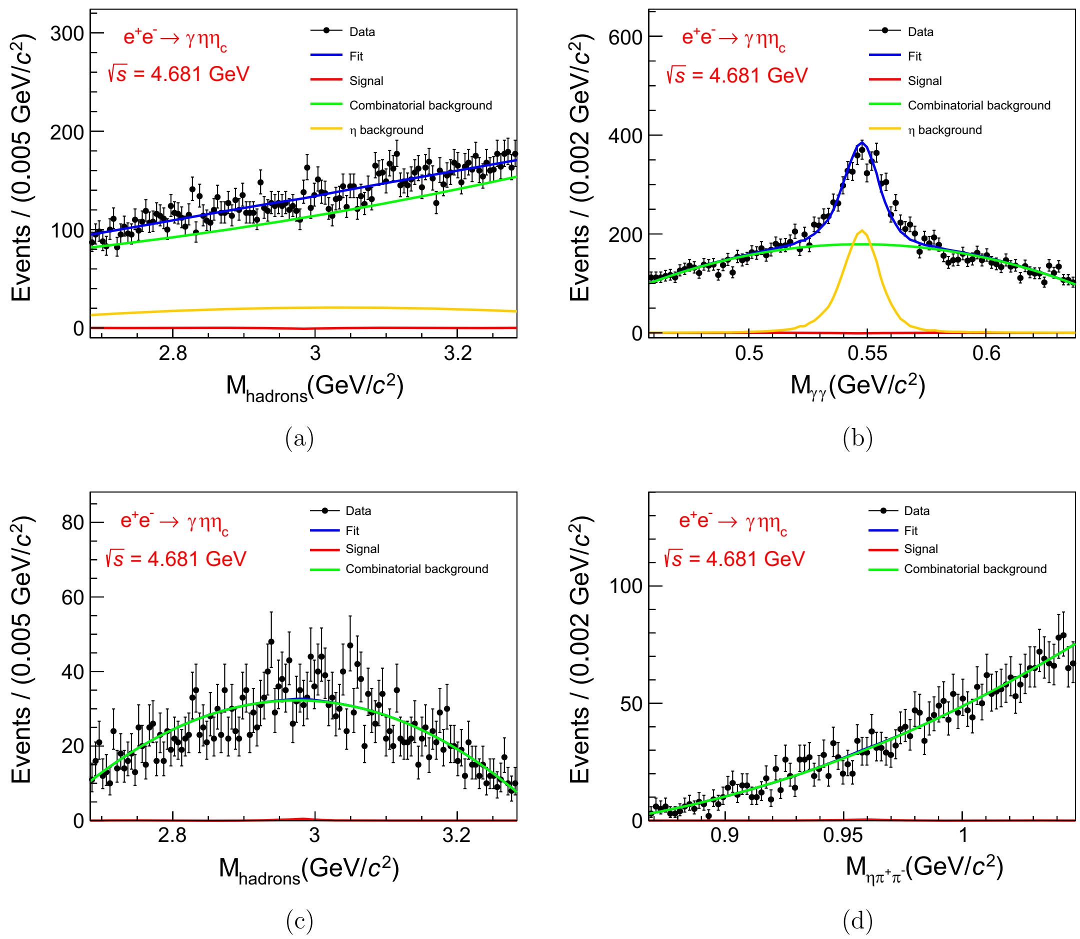


FIG. 3. Fits to the invariant mass distributions of (a, c) $M_{\mathrm{hadrons}}$, (b) $M_{\gamma\gamma}$, and (d) $M_{\eta\pi^+\pi^-}$ at $\sqrt{s} = 4.681$ GeV. The black dots with error bars are data, the red solid lines are the MC signals, the green solid lines are the flat background, and the orange solid lines indicate the background containing $\eta$.

events containing $\eta$ mesons. These backgrounds are considered in the two-dimensional fit, as shown in Sec. IV.

## IV. SIGNAL YIELD EXTRACTION

The signal yield of the $e^+e^- \to \gamma\eta^{(\prime)}\eta_c$ process is determined through an unbinned maximum likelihood fit to the two-dimensional distribution of $M_{\gamma\gamma(\eta\pi^+\pi^-)}$ versus $M_{\mathrm{hadrons}}$. The fit ranges are set as follows: $[0.458, 0.638]$ GeV$/c^2$ (for $M_{\gamma\gamma}$), $[0.868, 1.048]$ GeV$/c^2$ (for $M_{\eta\pi^+\pi^-}$), and $[2.684, 3.284]$ GeV$/c^2$ (for $M_{\mathrm{hadrons}}$). The signal is described by a combination of 16 weighted shapes obtained from the signal MC, where the weight is $\frac{\mathcal{B}_i\epsilon_i}{\sum_i \mathcal{B}_i\epsilon_i}$. Here, $\mathcal{B}_i$ denotes the branching fraction of the $\eta_c$ decay to the $i$th decay mode, and $\epsilon_i$ represents the detection efficiency obtained from MC samples.

For the $e^+e^- \to \gamma\eta\eta_c$ process, the backgrounds are modeled using two distinct components, each described by a two-dimensional probability density function (PDF). The first component, corresponding to backgrounds containing only $\eta$, is parametrized using the MC shape of $\eta$ in the $M_{\gamma\gamma}$ distribution, obtained from the MC sample, combined with a second-order Chebyshev polynomial in the $M_{\mathrm{hadrons}}$ distribution. The second component, representing the remaining backgrounds, is described by a two-dimensional second-order Chebyshev polynomial. For the $e^+e^- \to \gamma\eta'\eta_c$ process, since there is no background containing $\eta'$, the background is described solely by a two-dimensional second-order Chebyshev polynomial. The two-dimensional fit results of $\eta_c$ and $\eta(\eta')$, projected onto the distributions of $M_{\mathrm{hadrons}}$ and $M_{\gamma\gamma(\eta\pi^+\pi^-)}$ at $\sqrt{s} = 4.681$ GeV, are shown in Fig. 3. The signal yield of $e^+e^- \to \gamma\eta^{(\prime)}\eta_c$ at $\sqrt{s} = 4.681$ GeV is $-9.9 \pm 40.0(5.2 \pm 11.2)$ with a statistical significance of $1.4\sigma(0.4\sigma)$. The significance is calculated from the change in the negative log-likelihood function lnL with and without assuming the presence of signal, while considering the change in degrees of freedom in the fits. The significance at other energy points is listed in Table I.

## V. UPPER LIMIT ON BORN CROSS SECTIONS

The Born cross sections of $e^+e^- \to \gamma\eta^{(\prime)}\eta_c$ are calculated by

$$\sigma^{\rm Born} = \frac{N^{\rm obs}}{\mathcal{L}\cdot(1+\delta)\cdot\frac{1}{|1-\Pi|^2}\cdot\mathcal{B}\cdot\epsilon}. \quad (1)$$

Here, $N^{\rm obs}$ is the signal yield, $\mathcal{L}$ is the integrated luminosity of the data sample taken at each c.m. energy, and $\frac{1}{|1-\Pi|^2}$ is the vacuum polarization factor [33]. For $e^+e^- \to \gamma\eta\eta_c$, $\mathcal{B}\cdot\epsilon = \mathcal{B}(\eta\to\gamma\gamma)\sum_i \mathcal{B}_i\epsilon_i$, while for $e^+e^- \to \gamma\eta'\eta_c$, $\mathcal{B}\cdot\epsilon = \mathcal{B}(\eta'\to\eta\pi^+\pi^-)\mathcal{B}(\eta\to\gamma\gamma)\sum_i \mathcal{B}_i\epsilon_i$, where $\mathcal{B}(\eta\to\gamma\gamma)$ and $\mathcal{B}(\eta'\to\eta\pi^+\pi^-)$ are the branching fractions of $\eta\to\gamma\gamma$ and $\eta'\to\eta\pi^+\pi^-$ taken from the PDG [30]. Then, $1+\delta$ is the radiative (ISR) correction factor, which is defined as

$$(1+\delta) = \frac{\int \sigma^{\rm dress}(s(1-x))F(x,s)dx}{\sigma^{\rm dress}(s)}. \quad (2)$$

Here, $F(x,s)$ is the radiator function, which is known from a QCD calculation with an accuracy of 0.1% [34], $s$ is the square of the c.m. energy, and $x = 2E_{\gamma\rm ISR}/\sqrt{s}$, where $E_{\gamma\rm ISR}$ is the energy of the ISR photon. The $\sigma^{\rm dress}(s)$ is the dressed cross section.

Since no significant $e^+e^- \to \gamma\eta^{(\prime)}\eta_c$ signal is observed, we set the upper limit at the 90% confidence level (C.L.) on $\sigma(e^+e^- \to \gamma\eta^{(\prime)}\eta_c)$, incorporating the systematic uncertainty and using the Bayesian method [35]. The likelihood that produces the most conservative upper limit is selected after considering the additive systematic terms. To incorporate the multiplicative terms into the Born cross section limit, the probability of the signal yield $P(N)$ determined using a maximum likelihood fit is convolved with a PDF of the sensitivity. The details of systematic uncertainties can be found in Sec. VI. The upper limits of the signal yields ($N^{\rm obs}_{\rm UL}$) at the 90% C.L. are determined by

$$0.9\int_0^\infty P(N)dN = \int_0^{N^{\rm obs}_{\rm UL}} P(N)dN. \quad (3)$$

Using Eq. (1), we set the upper limits on the Born cross sections for $e^+e^- \to \gamma\eta^{(\prime)}\eta_c$ at 90% C.L. The results are summarized in Table I.

## VI. SYSTEMATIC UNCERTAINTY

The sources of systematic uncertainties are categorized into two types: additive and multiplicative terms. The additive uncertainties arise from the fit range, signal shape, background shape, and the difference between the MC sample and data. A conservative approach is adopted by considering all possible variations and selecting the one that yields the largest upper limit, as follows:

(i) The systematic uncertainty arising from the fit range is determined by varying the fit ranges of $M_{\gamma\gamma(\eta\pi^+\pi^-)}$ and $M_{\rm hadrons}$ by $\pm 5$ MeV$/c^2$ and $\pm 10$ MeV$/c^2$.

(ii) The nominal mass and width of $\eta_c$ are 2984.1 MeV$/c^2$ and 30.5 MeV, respectively [30]. The uncertainty associated with the $\eta_c$ shape is estimated by changing its mass and width parameters within their uncertainties.

(iii) The uncertainty due to the background shape is estimated by replacing the function from the second-order Chebyshev polynomial with both the first-order and the third-order Chebyshev polynomials.

(iv) The uncertainty due to the difference of mass resolution between data and MC simulation is estimated by convolving a Gaussian function to $\eta_c$ signal shape, where the mean value is varied by $\pm 1$ MeV$/c^2$, and the standard derivation is varied by 1, 2, and 3 MeV$/c^2$. For the $e^+e^- \to \gamma\eta\eta_c$ process, the $\eta$ signal shape is convolved with a Gaussian function parametrized by free parameters.

The multiplicative systematic uncertainty is considered by convolving a Gaussian function to the likelihood distribution. These uncertainties include the following sources:

(i) The integrated luminosity is determined using Bhabha scattering events, with a relative uncertainty of 1.0% uniformly assigned to all the measured energy points [16,17].

(ii) The systematic uncertainty of the ISR correction factor $1+\delta$ is estimated by comparing the difference between factors obtained by the flat line shape and $\psi(4660)$, with mass set to 4641 MeV$/c^2 \pm 5$, 10 MeV$/c^2$, and width to 73 MeV $\pm 5$, 10 MeV$/c^2$.

(iii) The parts of the Born cross sections' uncertainties associated with the branching fraction are calculated by $\frac{\sqrt{\sum_{i=1}^{16}(\epsilon_i\cdot\delta\mathcal{B}_i)^2}}{\sum_{i=1}^{16}(\epsilon_i\cdot\mathcal{B}_i)}$, where $\delta\mathcal{B}_i$ is the total branching fraction uncertainty after error propagation. The uncertainties of the branching fractions of $\eta_c \to$ hadrons are obtained from the BESIII measurement result [36], and the others are from the PDG [30].

(iv) The uncertainty from tracking or PID for charged tracks is determined to be 1.0% per track using the control samples $J/\psi \to \pi^+\pi^-\pi^0$, $J/\psi \to p\bar{p}\pi^+\pi^-$, and $J/\psi \to K^0_S K^\pm\pi^\mp$ + c.c. [37].

(v) The systematic uncertainty due to the photon detection is assigned as 1.0% per photon by analyzing the control samples $J/\psi \to \rho^0\pi^0$ and $e^+e^- \to \gamma\gamma$ [38].

(vi) The systematic uncertainty due to the $K^0_S$ reconstruction is studied using control samples $J/\psi \to K^{*\pm}K^\mp$ and $J/\psi \to \phi K^0_S K^\pm\pi^\mp$, and estimated to be 1.0% [39].

TABLE II. Relative systematic uncertainties (%) on $\sigma^{\rm Born}(e^+e^- \to \gamma\eta^{(\prime)}\eta_c)$ at $\sqrt{s} = 4.681$ GeV.

| Source | | $\sigma^{\rm Born}(e^+e^- \to \gamma\eta\eta_c)$ | $\sigma^{\rm Born}(e^+e^- \to \gamma\eta'\eta_c)$ |
|---|---|---|---|
| Luminosity | | 1.0 | 1.0 |
| ISR correction | | 3.3 | 0.9 |
| $\sum_i \mathcal{B}_i\epsilon_i$ | $\mathcal{B}_{\eta_c\to X_i}$ | 18.1 | 18.1 |
| | Tracking | 3.3 | 5.1 |
| | Photon selection | 3.0 | 3.1 |
| | PID | 3.3 | 5.1 |
| | $K_S^0$ reconstruction | 0.1 | 0.1 |
| | $\pi^0$ reconstruction | 0.4 | 0.4 |
| | $\eta$ reconstruction | 0.3 | 0.3 |
| | Kinematic fit | 1.1 | 1.0 |
| | Contamination | 1.2 | 0.6 |
| Total | | 19.3 | 19.9 |

(vii) Using a high-purity control sample of $J/\psi \to \pi^0 p\bar{p}$ or $J/\psi \to \eta p\bar{p}$, the systematic uncertainty from the $\pi^0$ or $\eta$ reconstruction is determined to be 1.0% [40].

(viii) The systematic uncertainty associated with the kinematic fit is assigned as the difference between the detection efficiencies before and after the helix parameter corrections [41] in the signal MC simulation.

(ix) The contamination among the 16 decay modes of $\eta_c$ is calculated by using the signal MC simulation.

Table II summarizes the multiplicative systematic uncertainties. All sources are treated as uncorrelated, and the total systematic uncertainty is obtained by adding them in quadrature.

## VII. SUMMARY

Based on $e^+e^-$ annihilation data corresponding to an integrated luminosity of 10.6 $\text{fb}^{-1}$ collected with the BESIII detector at the BEPCII collider for c.m. energies in the range $\sqrt{s} = 4.258$–$4.681$ GeV, we searched for the $1^{-+}$ charmoniumlike hybrid via $e^+e^- \to \gamma\eta^{(\prime)}\eta_c$ for the first time. No significant signal was observed, and the upper limits at the 90% C.L. on the Born cross sections for $e^+e^- \to \gamma\eta\eta_c$ and $e^+e^- \to \gamma\eta'\eta_c$ were determined. Some theoretical calculations also predict that $\eta_{c1}$ can decay to the open-charm final states, such as $D_1\bar{D}$, $D^*\bar{D}$ and $D^*\bar{D}^*$ [15]. With future datasets of higher statistics, searches for the $\eta_{c1}$ in these final states can be further explored.

## ACKNOWLEDGMENTS

BESIII Collaboration thanks the staff of BEPCII and the IHEP computing center for their strong support. This work is supported in part by the National Key R&D Program of China under Contracts No. 2020YFA0406300, No. 2020YFA0406400, No. 2023YFA1606000, and No. 2023YFA1606704; the National Natural Science Foundation of China (NSFC) under Contracts No. 11635010, No. 11935015, No. 11935016, No. 11935018, No. 12025502, No. 12035009, No. 12035013, No. 12061131003, No. 12192260, No. 12192261, No. 12192262, No. 12192263, No. 12192264, No. 12192265, No. 12221005, No. 12225509, No. 12235017, and No. 12361141819; the Chinese Academy of Sciences (CAS) Large-Scale Scientific Facility Program; CAS under Contract No. YSBR-101; the 100 Talents Program of CAS; The Institute of Nuclear and Particle Physics (INPAC) and Shanghai Key Laboratory for Particle Physics and Cosmology; Agencia Nacional de Investigación y Desarrollo de Chile (ANID), Chile, under Contract No. ANID PIA/APOYO AFB230003; the German Research Foundation DFG under Contract No. FOR5327; Istituto Nazionale di Fisica Nucleare, Italy; Knut and Alice Wallenberg Foundation under Contracts No. 2021.0174 and No. 2021.0299; the Ministry of Development of Turkey under Contract No. DPT2006K-120470; the National Research Foundation of Korea under Contract No. NRF-2022R1A2C1092335; the National Science and Technology fund of Mongolia; the National Science Research and Innovation Fund (NSRF) via the Program Management Unit for Human Resources and Institutional Development, Research and Innovation of Thailand, under Contract No. B50G670107; the Swedish Research Council under Contract No. 2019.04595; the U.S. Department of Energy under Contract No. DE-FG02-05ER41374.

## DATA AVAILABILITY

The data that support the findings of this article are not publicly available upon publication because it is not technically feasible and/or the cost of preparing, depositing, and hosting the data would be prohibitive within the terms of this research project. The data are available from the authors upon reasonable request.

## APPENDIX

Figures 4–8 display the distributions of $M_{\gamma\gamma}$ versus $M_{\mathrm{hadrons}}$, $M_{\mathrm{hadrons}}$, and $M_{\gamma\gamma}$ for each data sample. Figures 9–12 display the distributions of $M_{\eta\pi^+\pi^-}$ versus $M_{\mathrm{hadrons}}$, $M_{\mathrm{hadrons}}$, $M_{\eta\pi^+\pi^-}$, and $M_{\gamma\gamma}$ for each data sample. Figures 13–16 are the fit results to the invariant mass distributions for each data sample.

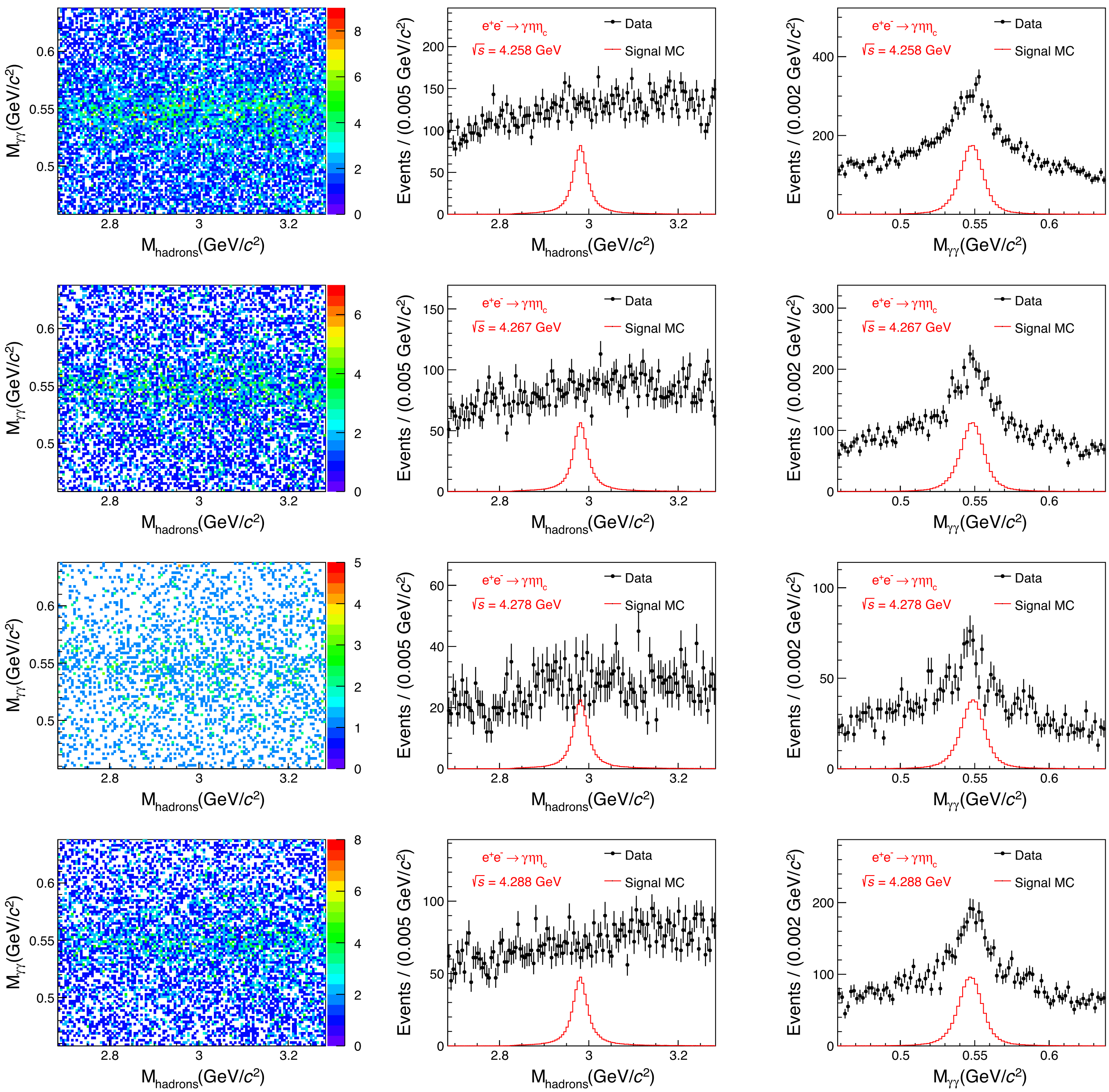


FIG. 4. The distributions of (left) $M_{\mathrm{hadrons}}$ versus $M_{\gamma\gamma}$, (middle) $M_{\mathrm{hadrons}}$, and (right) $M_{\gamma\gamma}$ for $e^+e^- \to \gamma\eta\eta_c$ candidate events. The rows show the distributions at $\sqrt{s} = 4.258$–$4.288$ GeV.

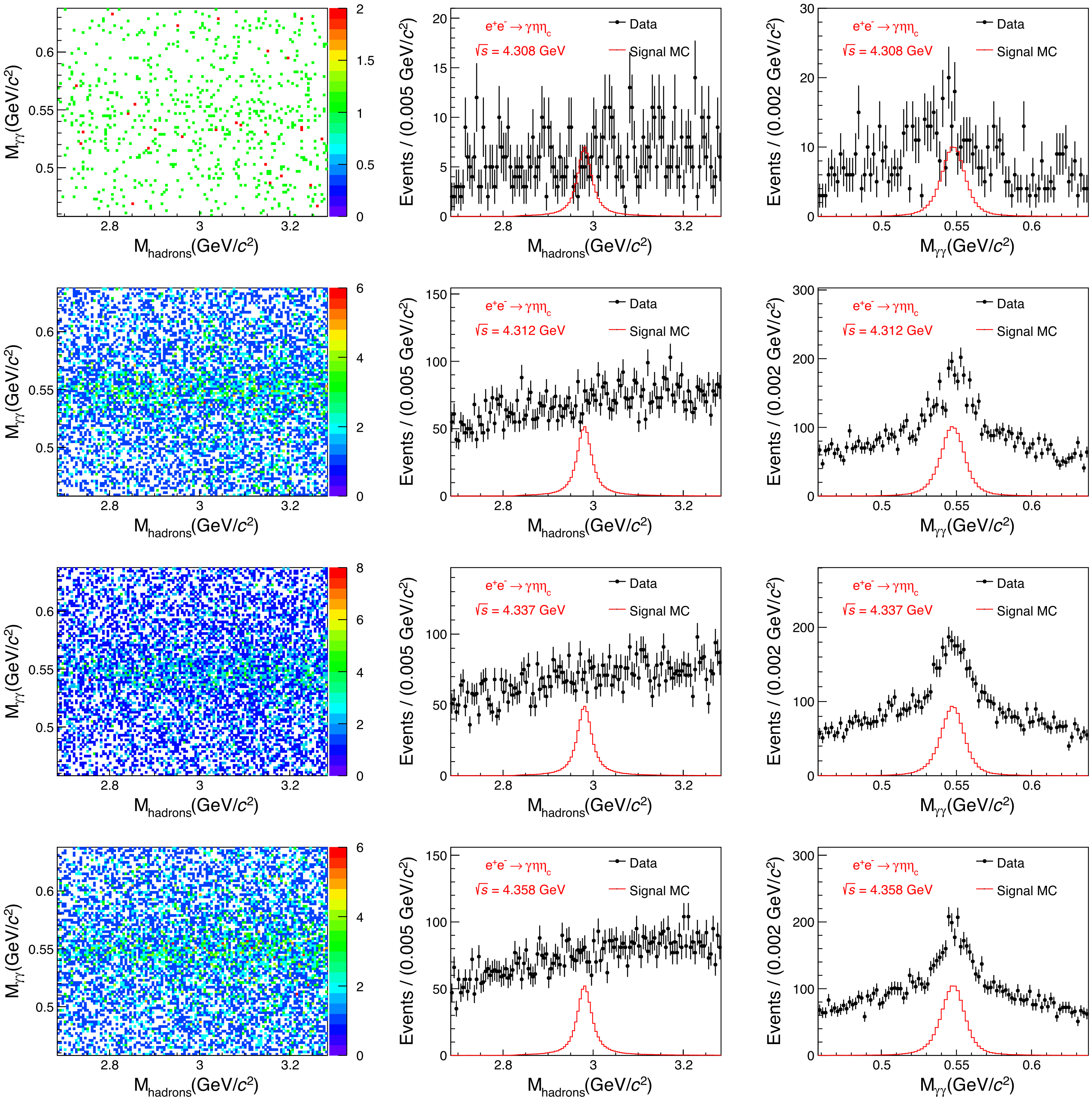


FIG. 5. The distributions of (left) $M_{\mathrm{hadrons}}$ versus $M_{\gamma\gamma}$, (middle) $M_{\mathrm{hadrons}}$, and (right) $M_{\gamma\gamma}$ for $e^+e^- \to \gamma\eta\eta_c$ candidate events. The rows show the distributions at $\sqrt{s} = 4.308$–$4.358$ GeV.

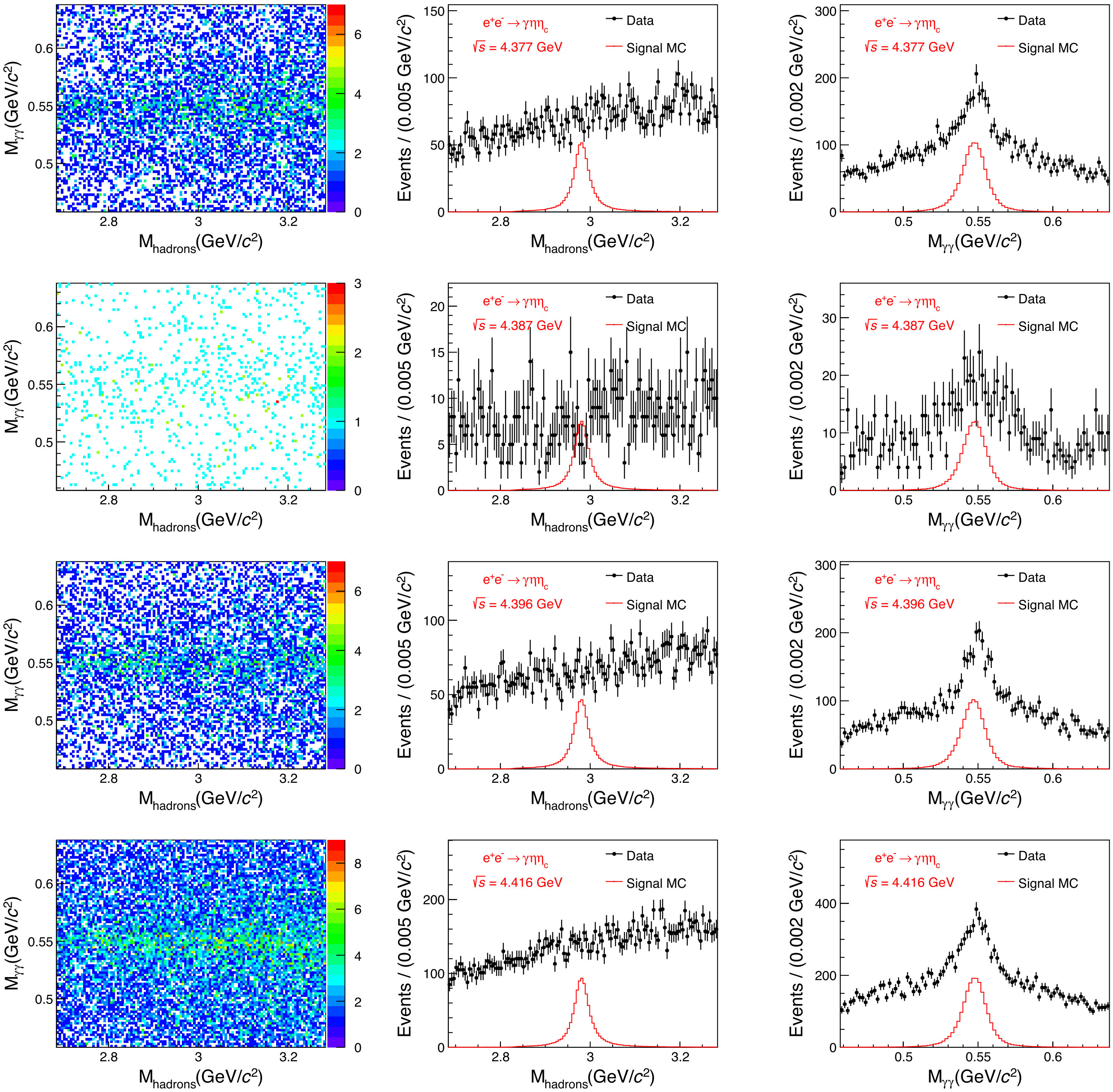


FIG. 6. The distributions of (left) $M_{\text{hadrons}}$ versus $M_{\gamma\gamma}$, (middle) $M_{\text{hadrons}}$, and (right) $M_{\gamma\gamma}$ for $e^+e^- \to \gamma\eta\eta_c$ candidate events. The rows show the distributions at $\sqrt{s} = 4.377$–$4.416$ GeV.

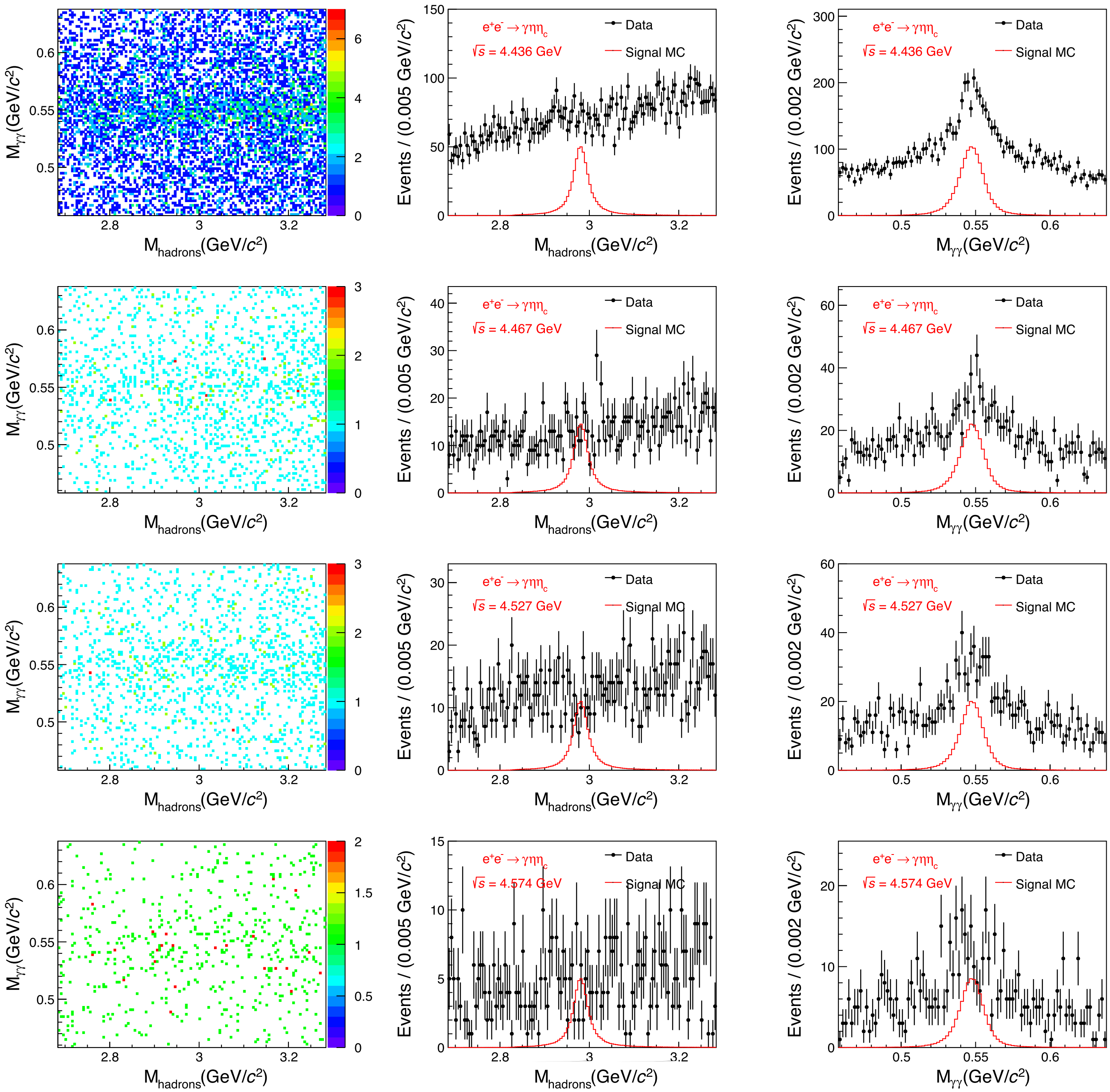


FIG. 7. The distributions of (left) $M_{\mathrm{hadrons}}$ versus $M_{\gamma\gamma}$, (middle) $M_{\mathrm{hadrons}}$, and (right) $M_{\gamma\gamma}$ for $e^+e^- \to \gamma\eta\eta_c$ candidate events. The rows show the distributions at $\sqrt{s} = 4.436$–$4.574$ GeV.

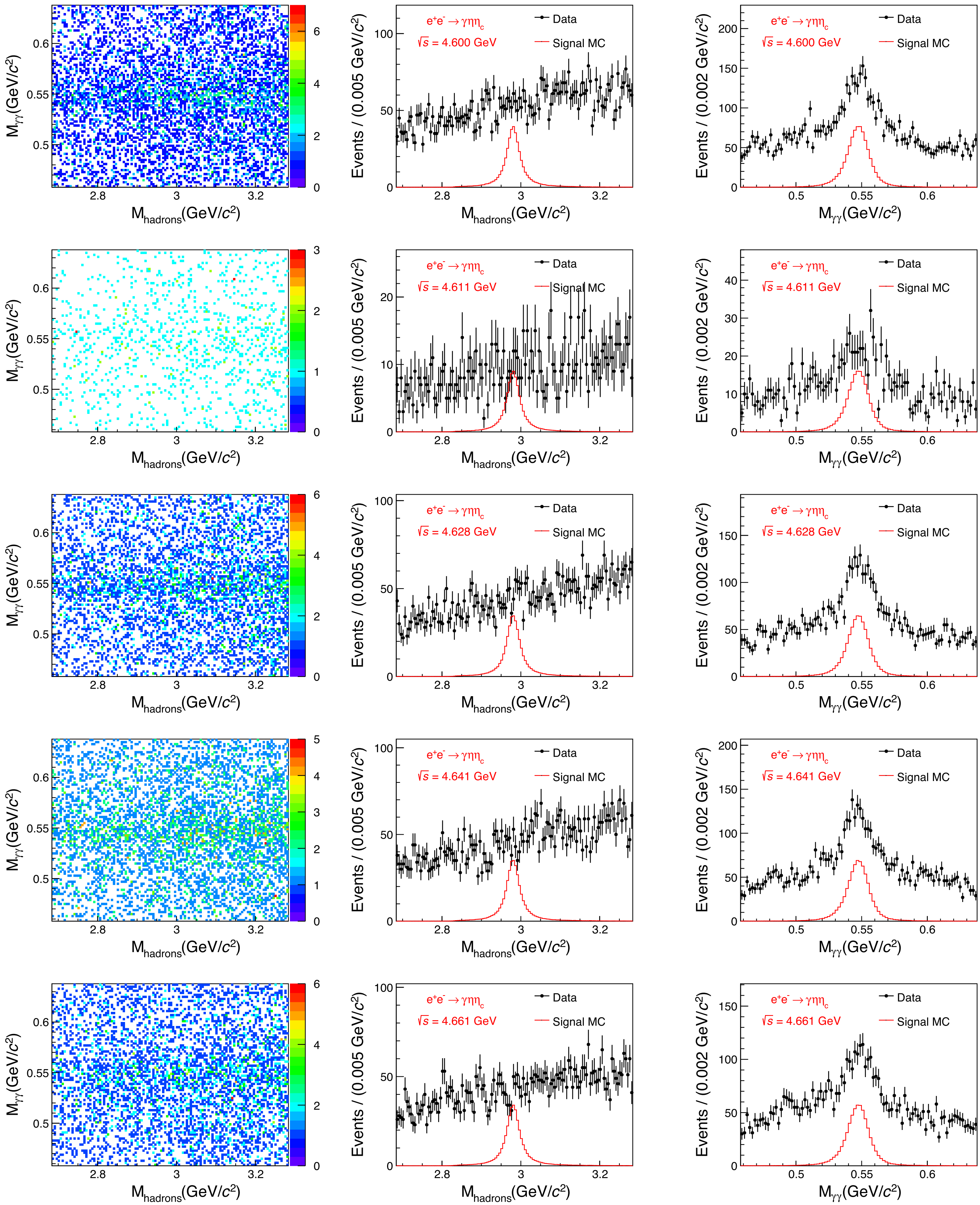


FIG. 8. The distributions of (left) $M_{\text{hadrons}}$ versus $M_{\gamma\gamma}$, (middle) $M_{\text{hadrons}}$, and (right) $M_{\gamma\gamma}$ for $e^+e^- \to \gamma\eta\eta_c$ candidate events. The rows show the distributions at $\sqrt{s} = 4.600$–$4.661$ GeV.

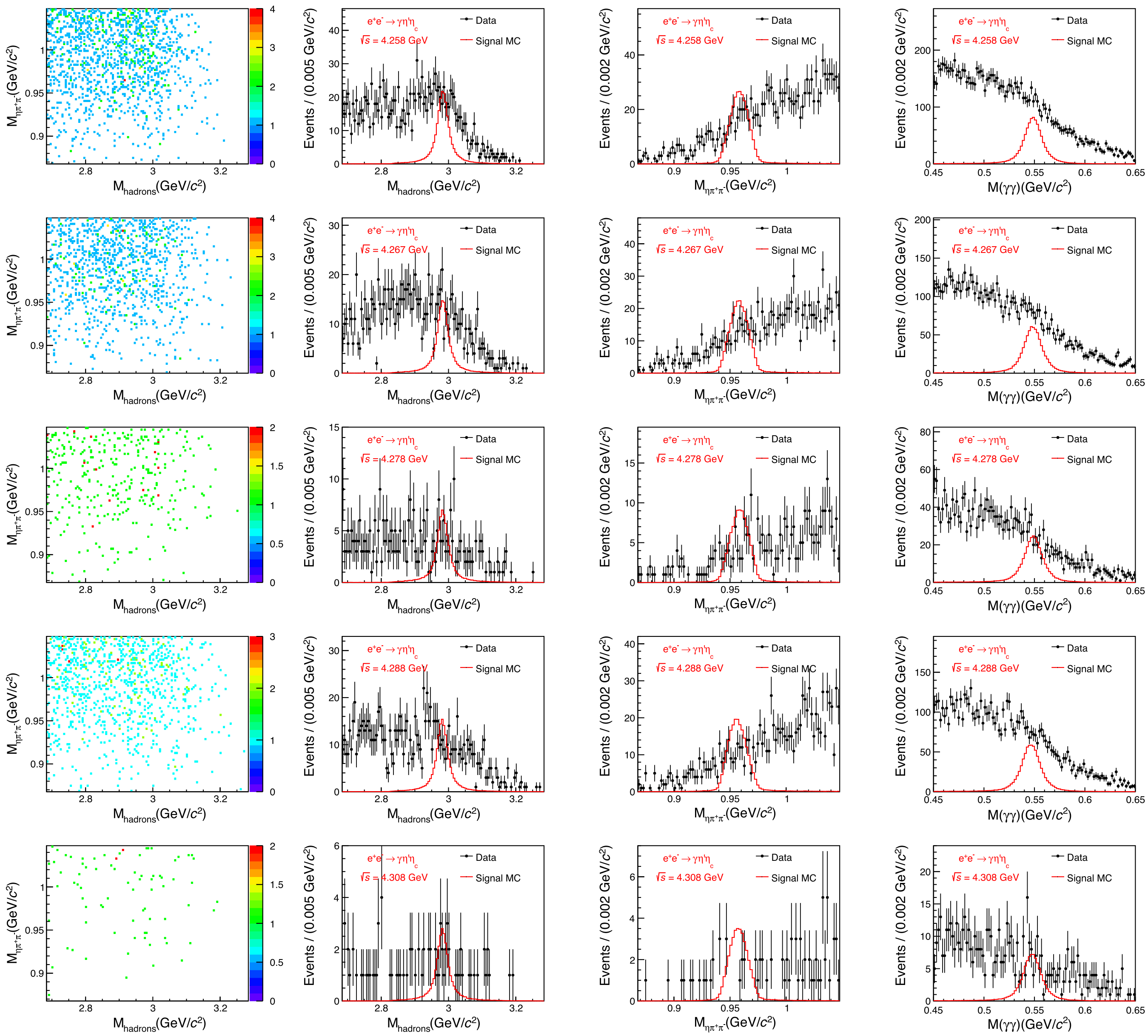


FIG. 9. The distributions of (left) $M_{\mathrm{hadrons}}$ versus $M_{\eta\pi^+\pi^-}$, (middle left) $M_{\mathrm{hadrons}}$, (middle right) $M_{\eta\pi^+\pi^-}$, and (right) $M_{\gamma\gamma}$ for $e^+e^- \to \gamma\eta'\eta_c$ candidate events. The rows show the distributions at $\sqrt{s} = 4.258$–$4.308$ GeV.

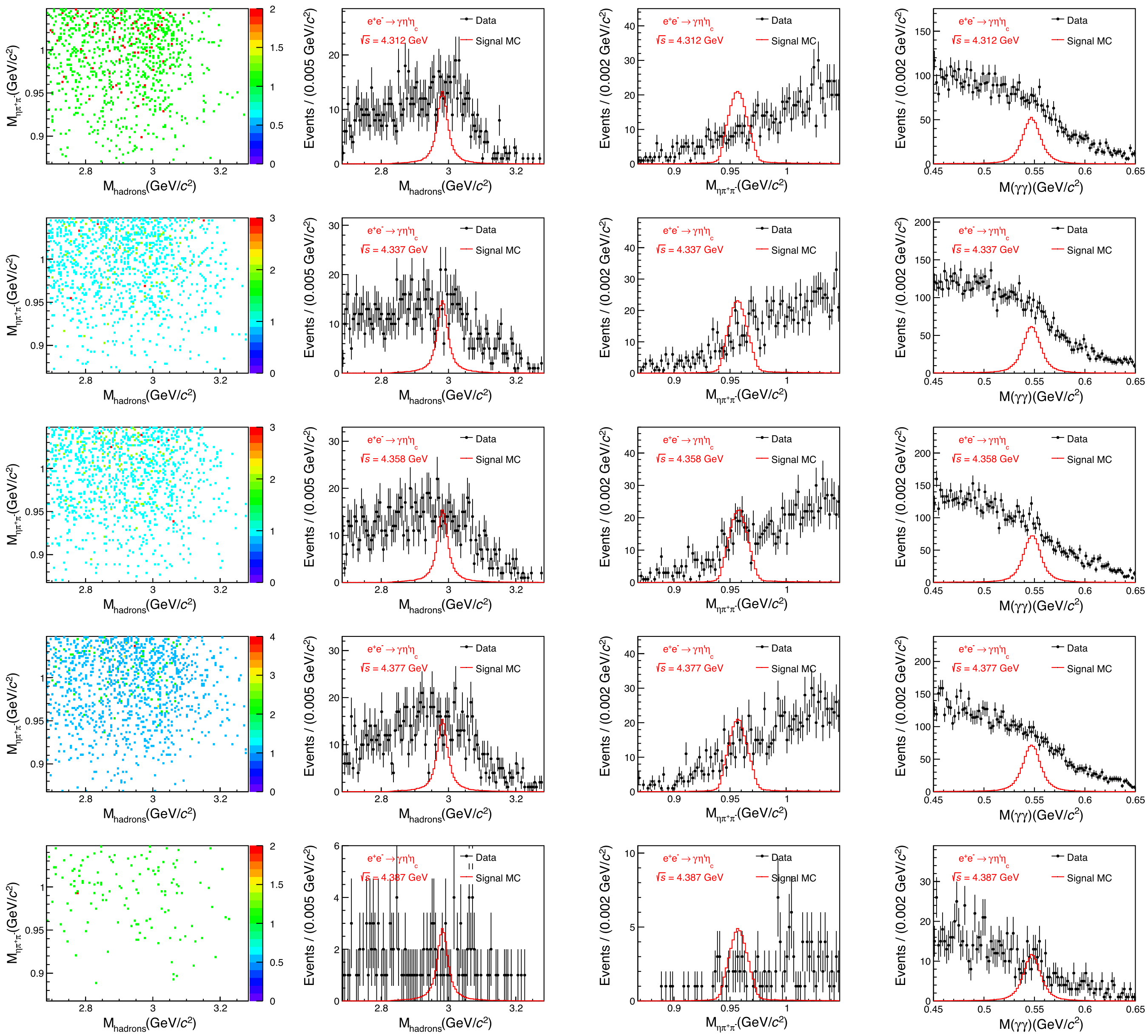

FIG. 10. The distributions of (left) $M_{\mathrm{hadrons}}$ versus $M_{\eta\pi^+\pi^-}$, (middle left) $M_{\mathrm{hadrons}}$, (middle right) $M_{\eta\pi^+\pi^-}$, and (right) $M_{\gamma\gamma}$ for $e^+e^- \to \gamma\eta'\eta_c$ candidate events. The rows show the distributions at $\sqrt{s} = 4.312$–$4.387$ GeV.

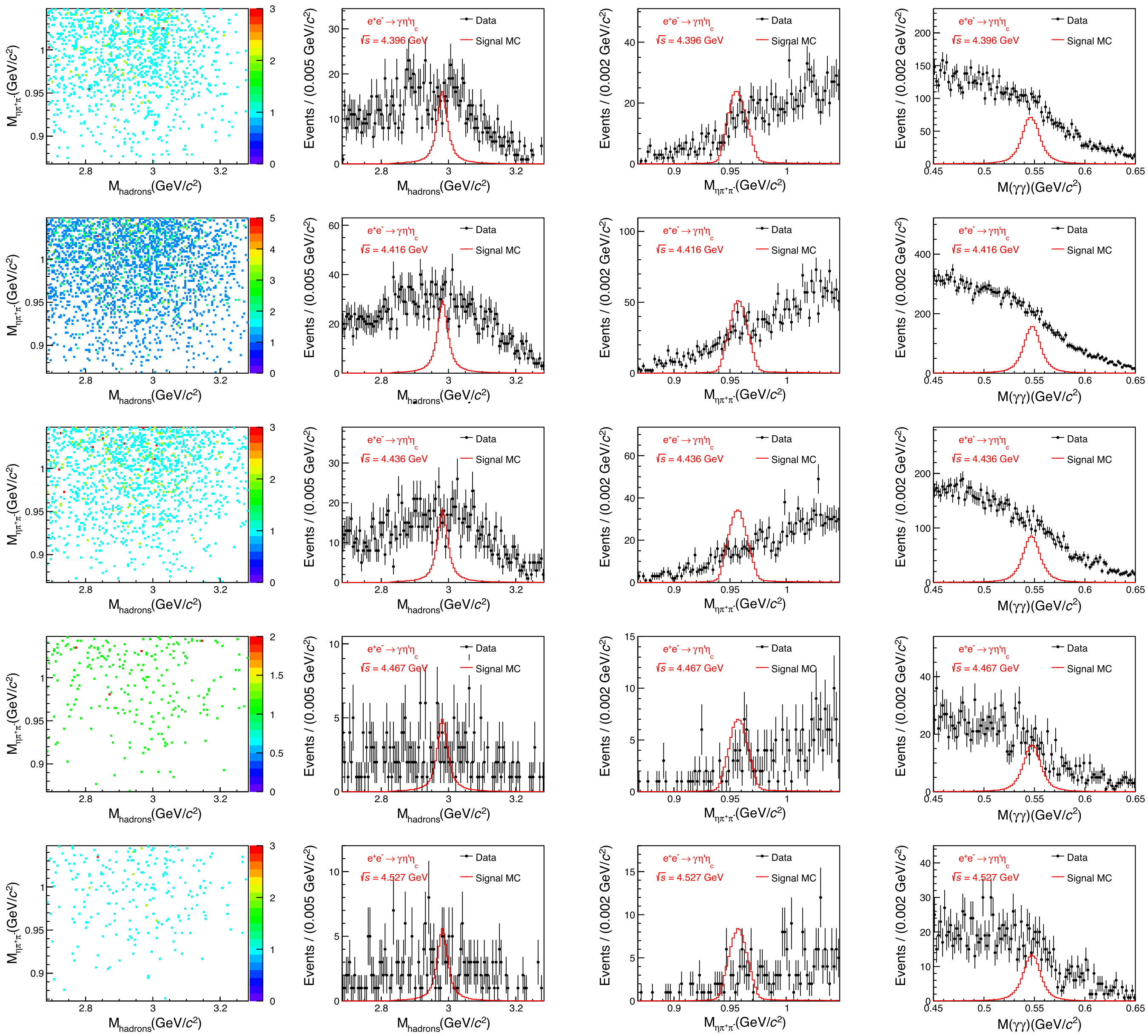

FIG. 11. The distributions of (left) $M_{\mathrm{hadrons}}$ versus $M_{\eta\pi^+\pi^-}$, (middle left) $M_{\mathrm{hadrons}}$, (middle right) $M_{\eta\pi^+\pi^-}$, and (right) $M_{\gamma\gamma}$ for $e^+e^- \to \gamma\eta'\eta_c$ candidate events. The rows show the distributions at $\sqrt{s} = 4.396$–$4.527$ GeV.

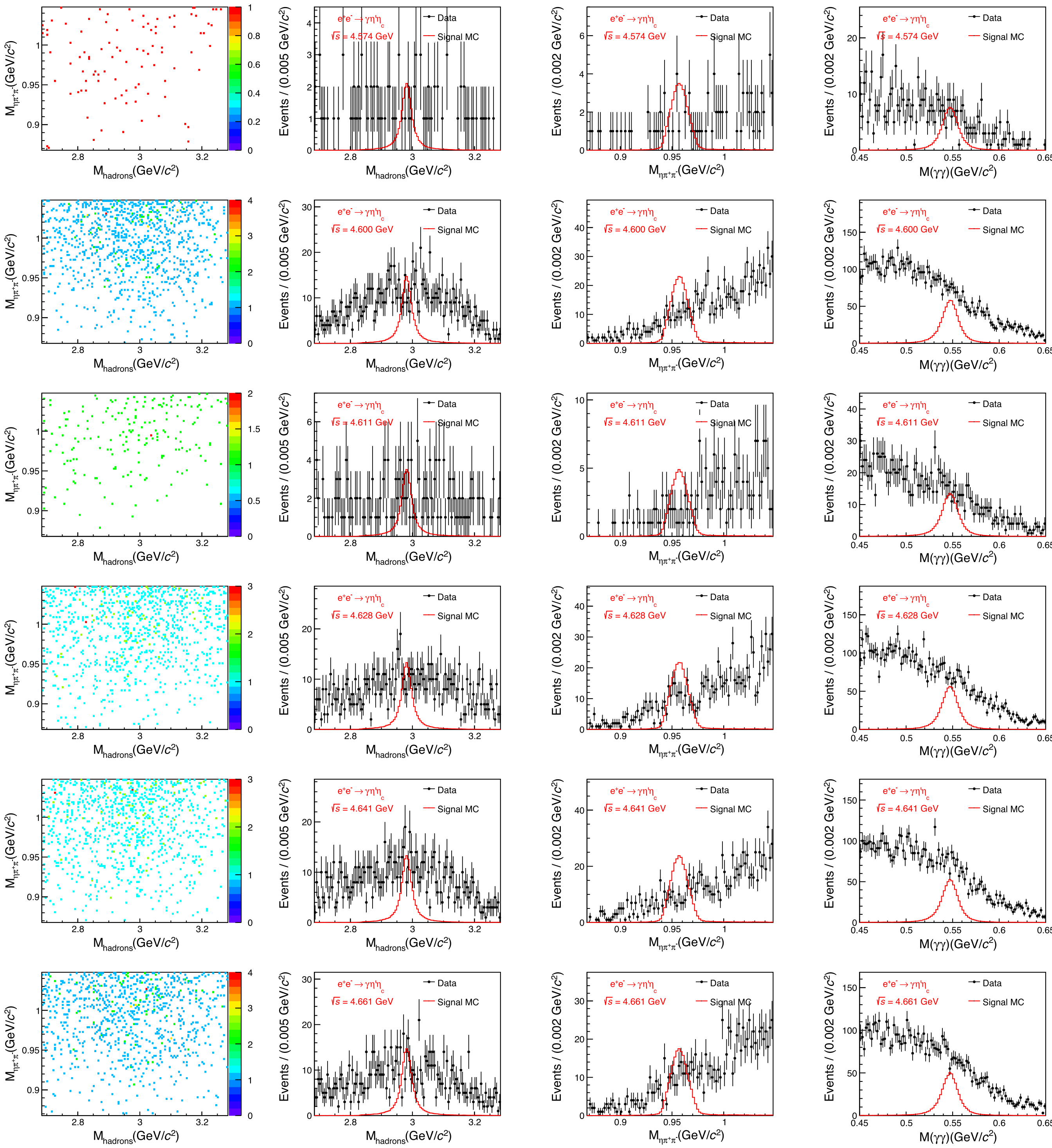

FIG. 12. The distributions of (left) $M_{\mathrm{hadrons}}$ versus $M_{\eta\pi^+\pi^-}$, (middle left) $M_{\mathrm{hadrons}}$, (middle right) $M_{\eta\pi^+\pi^-}$, and (right) $M_{\gamma\gamma}$ for $e^+e^- \to \gamma\eta'\eta_c$ candidate events. The rows show the distributions at $\sqrt{s} = 4.574$–$4.661$ GeV.

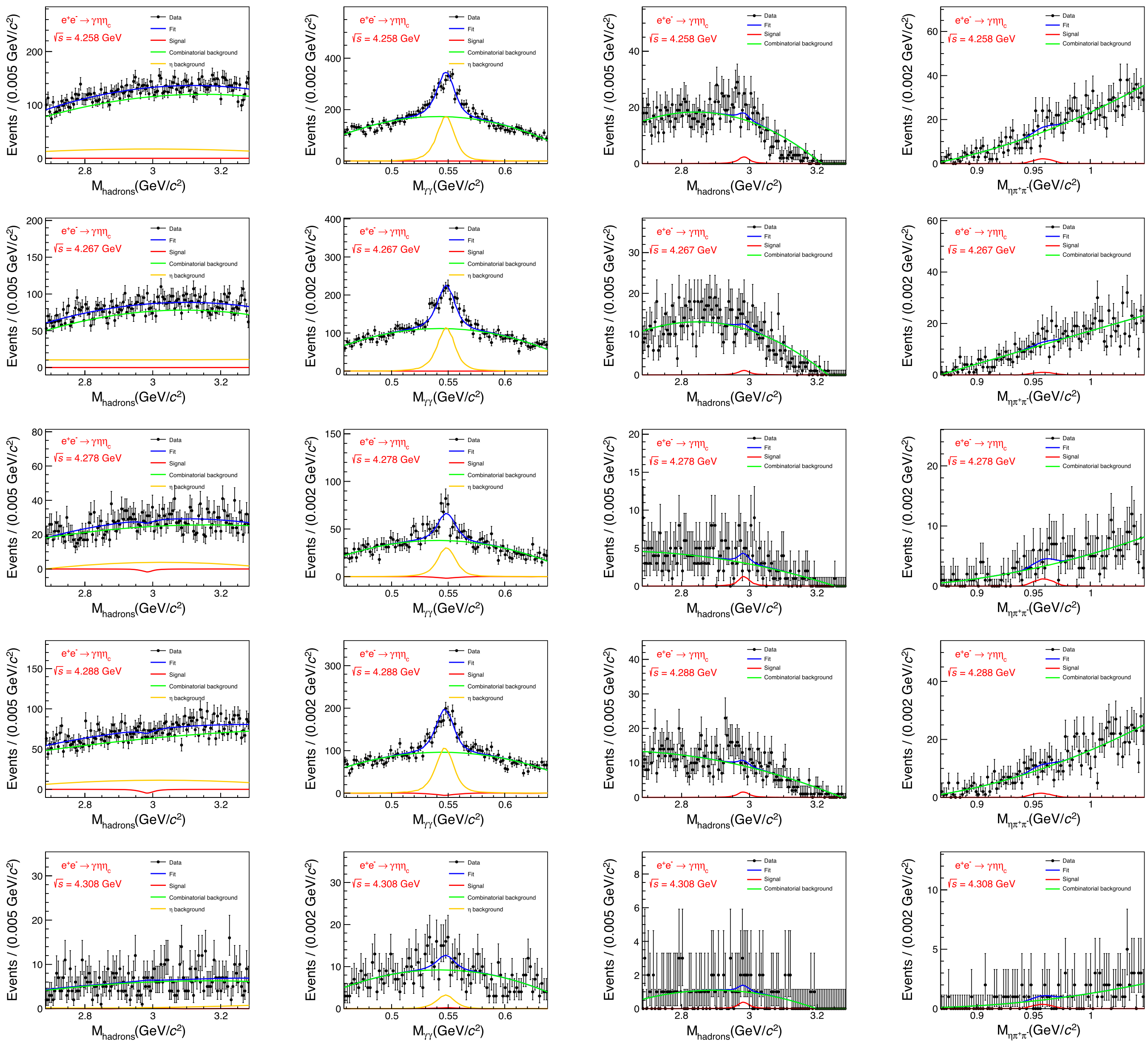


FIG. 13. Fits to the invariant mass distributions of (left) $M_{\mathrm{hadrons}}$ and (middle left) $M_{\gamma\gamma}$ for $e^+e^- \to \gamma\eta\eta_c$ candidate events, and (middle right) $M_{\mathrm{hadrons}}$ and (right) $M_{\eta\pi^+\pi^-}$ for $e^+e^- \to \gamma\eta'\eta_c$ candidate events. The rows show the distributions at $\sqrt{(s)} = 4.258$–$4.308$ GeV.

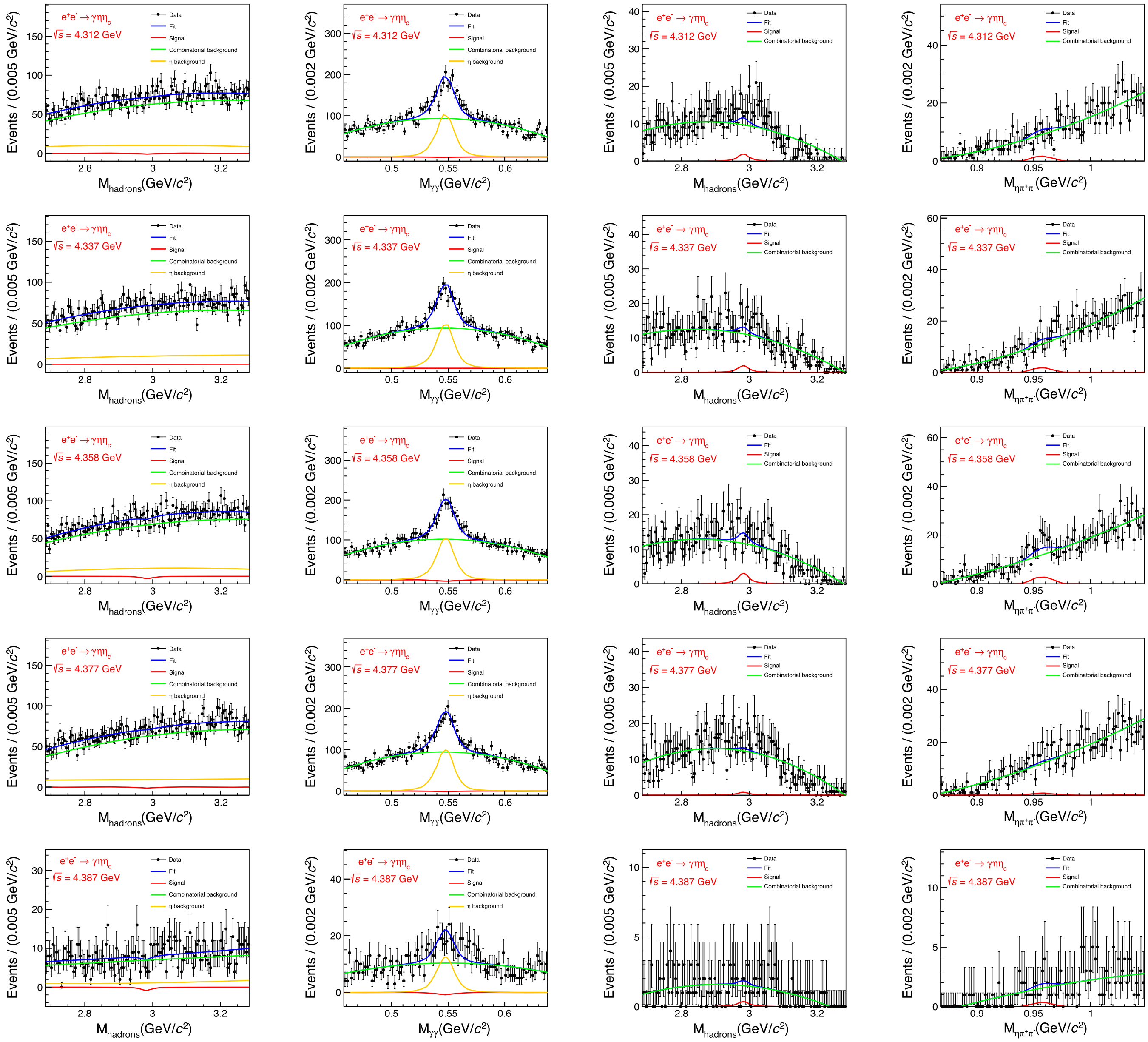


FIG. 14. Fits to the invariant mass distributions of (left) $M_{\mathrm{hadrons}}$ and (middle left) $M_{\gamma\gamma}$ for $e^+e^- \to \gamma\eta\eta_c$ candidate events, and (middle right) $M_{\mathrm{hadrons}}$ and (right) $M_{\eta\pi^+\pi^-}$ for $e^+e^- \to \gamma\eta'\eta_c$ candidate events. The rows show the distributions at $\sqrt{(s)} = 4.312$–$4.387$ GeV.

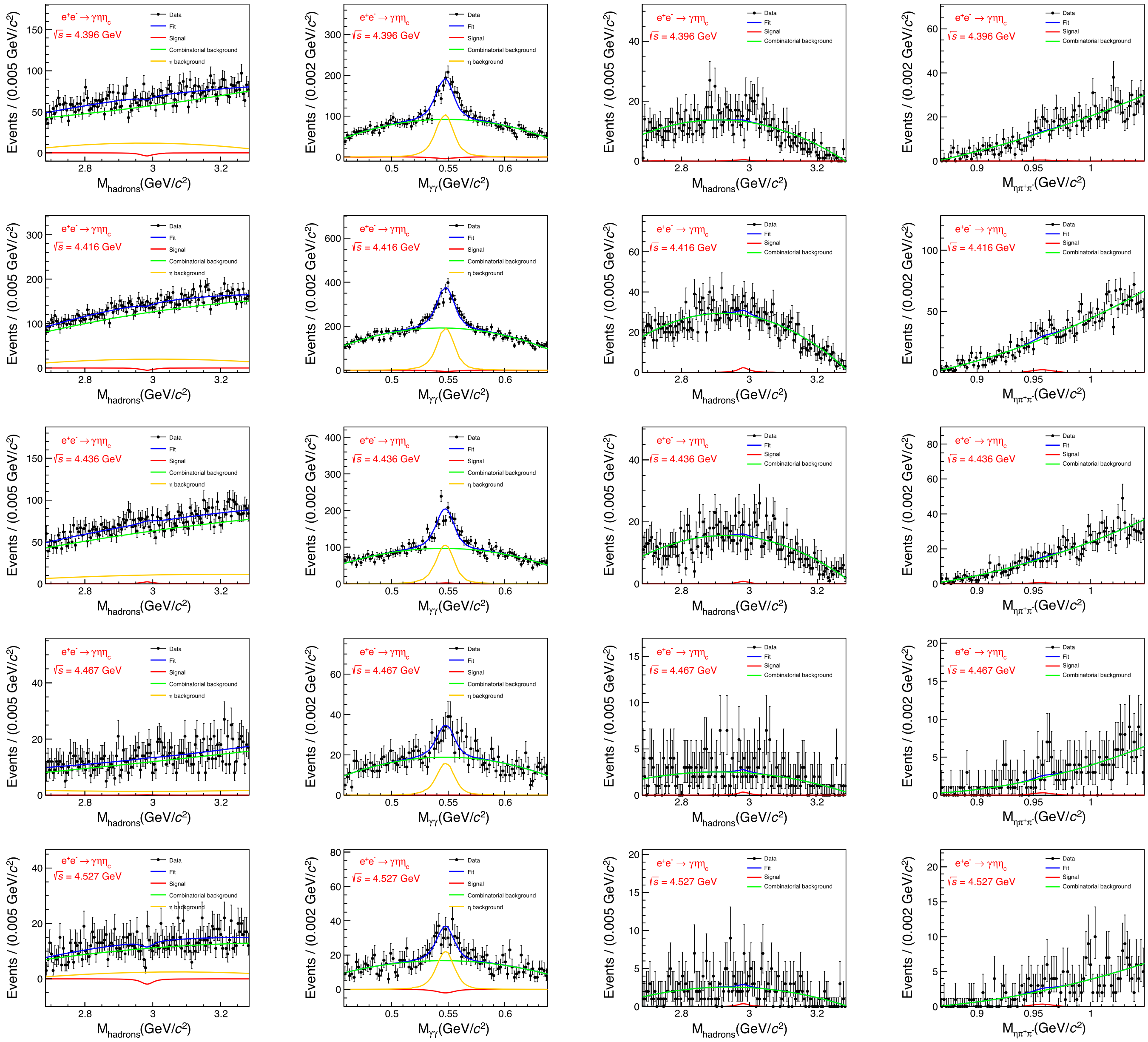


FIG. 15. Fits to the invariant mass distributions of (left) $M_{\mathrm{hadrons}}$ and (middle left) $M_{\gamma\gamma}$ for $e^+e^- \to \gamma\eta\eta_c$ candidate events, and (middle right) $M_{\mathrm{hadrons}}$ and (right) $M_{\eta\pi^+\pi^-}$ for $e^+e^- \to \gamma\eta'\eta_c$ candidate events. The rows show the distributions at $\sqrt{(s)} = 4.396$–$4.527$ GeV.

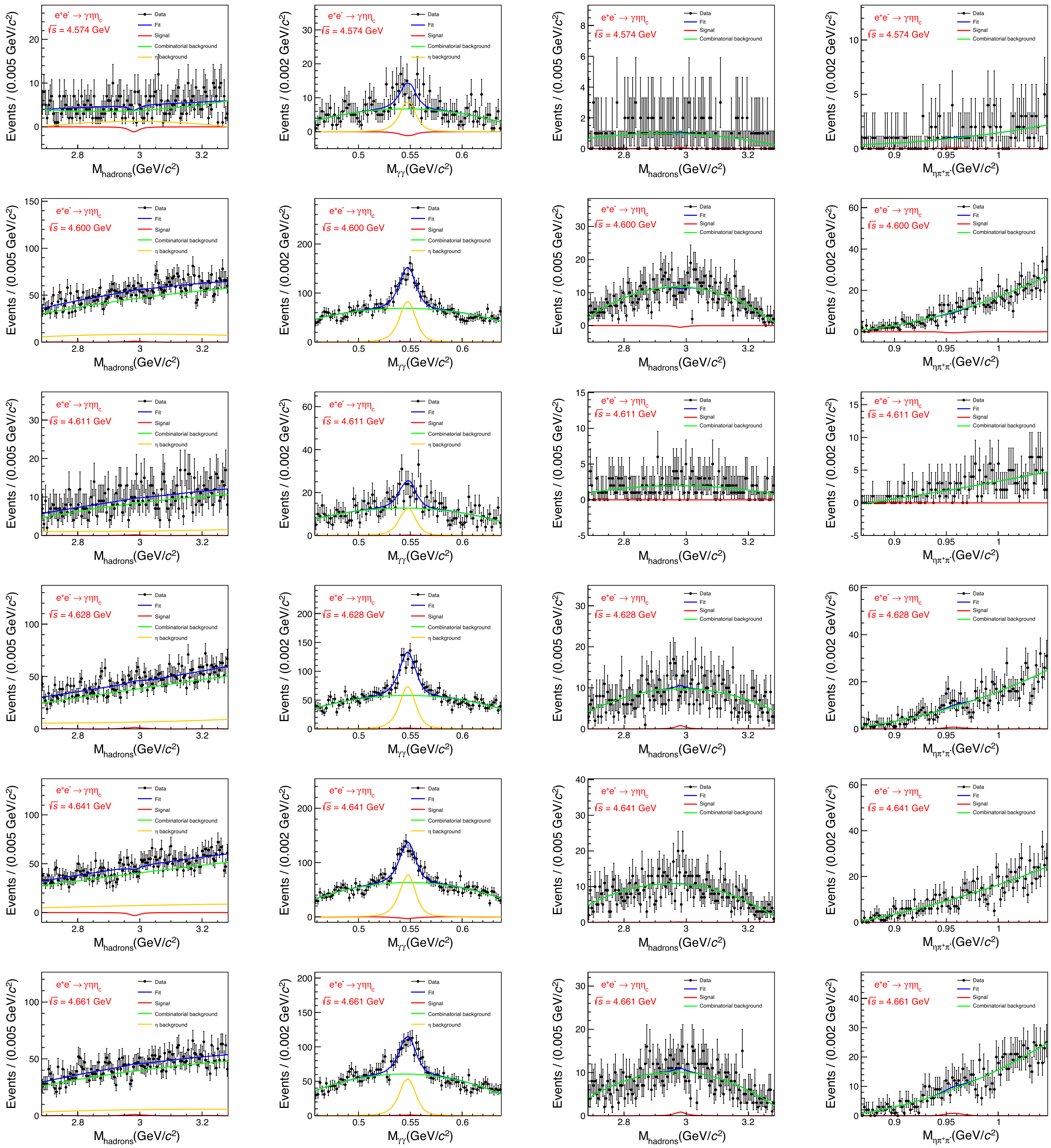

FIG. 16. Fits to the invariant mass distributions of (left) $M_{\mathrm{hadrons}}$ and (middle left) $M_{\gamma\gamma}$ for $e^+e^- \to \gamma\eta\eta_c$ candidate events, and (middle right) $M_{\mathrm{hadrons}}$ and (right) $M_{\eta\pi^+\pi^-}$ for $e^+e^- \to \gamma\eta'\eta_c$ candidate events. The rows show the distributions at $\sqrt{(s)} = 4.574$–$4.661$ GeV.

[1] J. J. Dudek, R. G. Edwards, P. Guo, and C. E. Thomas (Hadron Spectrum Collaboration), Phys. Rev. D **88**, 094505 (2013).
[2] L. Liu, G. Moir, M. Peardon, S. M. Ryan, C. E. Thomas, P. Vilaseca, J. J. Dudek, R. G. Edwards, B. Joó, and D. G. Richards, J. High Energy Phys. 07 (2012) 126.
[3] N. Brambilla, W. K. Lai, A. Mohapatra, and A. Vairo, Phys. Rev. D **107**, 054034 (2023).
[4] N. Brambilla, S. Eidelman, C. Hanhart, A. Nefediev, C.-P. Shen, C. E. Thomas, A. Vairo, and C.-Z. Yuan, Phys. Rep. **873**, 1 (2020).
[5] R. L. Workman *et al.* (Particle Data Group), Prog. Theor. Exp. Phys. **2022**, 083C01 (2022).
[6] S. L. Olsen, T. Skwarnicki, and D. Zieminska, Rev. Mod. Phys. **90**, 015003 (2018).
[7] C.-Z. Yuan, Natl. Sci. Rev. **8**, nwab182 (2021).
[8] C. A. Meyer and Y. Van Haarlem, Phys. Rev. C **82**, 025208 (2010).
[9] E. Klempt and A. Zaitsev, Phys. Rep. **454**, 1 (2007).
[10] A. Rodas *et al.* (JPAC Collaboration), Phys. Rev. Lett. **122**, 042002 (2019).
[11] A. J. Woss, J. J. Dudek, R. G. Edwards, C. E. Thomas, and D. J. Wilson (Hadron Spectrum Collaboration), Phys. Rev. D **103**, 054502 (2021).
[12] M. Ablikim *et al.* (BESIII Collaboration), Phys. Rev. D **106**, 072012 (2022); **107**, 079901(E) (2023).
[13] M. Ablikim *et al.* (BESIII Collaboration), Phys. Rev. Lett. **129**, 192002 (2022); **130**, 159901(E) (2023).
[14] X.-K. Dong, Y.-H. Lin, and B.-S. Zou, Phys. Rev. D **101**, 076003 (2020).
[15] C. Shi, Y. Chen, M. Gong, X. Jiang, Z. Liu, and W. Sun, Phys. Rev. D **109**, 094513 (2024).
[16] M. Ablikim *et al.* (BESIII Collaboration), Chin. Phys. C **39**, 093001 (2015).
[17] M. Ablikim *et al.* (BESIII Collaboration), Chin. Phys. C **46**, 113003 (2022).
[18] M. Ablikim *et al.* (BESIII Collaboration), Nucl. Instrum. Methods Phys. Res., Sect. A **614**, 345 (2010).
[19] C. Yu *et al.*, in *Proceedings of the 7th International Particle Accelerator Conference* (2016), p. TUYA01.
[20] M. Ablikim *et al.* (BESIII Collaboration), Chin. Phys. C **44**, 040001 (2020).
[21] J.-W. Zhang *et al.*, Radiat. Detect. Technol. Methods **6**, 289 (2022).
[22] X. Li *et al.*, Radiat. Detect. Technol. Methods **1**, 13 (2017).
[23] Y.-X. Guo *et al.*, Radiat. Detect. Technol. Methods **1**, 15 (2017).
[24] P. Cao *et al.*, Nucl. Instrum. Methods Phys. Res., Sect. A **953**, 163053 (2020).
[25] S. Agostinelli *et al.*, Nucl. Instrum. Methods Phys. Res., Sect. A **506**, 250 (2003).
[26] S. Jadach, B. F. L. Ward, and Z. Was, Comput. Phys. Commun. **130**, 260 (2000).
[27] S. Jadach, B. F. L. Ward, and Z. Was, Phys. Rev. D **63**, 113009 (2001).
[28] D. J. Lange, Nucl. Instrum. Methods Phys. Res., Sect. A **462**, 152 (2001).
[29] P. Rong-Gang, Chin. Phys. C **32**, 599 (2008).
[30] S. Navas *et al.* (Particle Data Group), Phys. Rev. D **110**, 030001 (2024).
[31] J. C. Chen, G. S. Huang, X. R. Qi, D. H. Zhang, and Y. S. Zhu, Phys. Rev. D **62**, 034003 (2000).
[32] E. Barberio, B. van Eijk, and Z. Was, Comput. Phys. Commun. **66**, 115 (1991).
[33] S. Actis *et al.* (Working Group on Radiative Corrections, Monte Carlo Generators for Low Energies), Eur. Phys. J. C **66**, 585 (2010).
[34] E. A. Kuraev and V. S. Fadin, Sov. J. Nucl. Phys. **41**, 466 (1985).
[35] J. Conrad, O. Botner, A. Hallgren, and C. Perez de los Heros, Phys. Rev. D **67**, 012002 (2003).
[36] M. Ablikim *et al.* (BESIII Collaboration), Phys. Rev. D **86**, 092009 (2012).
[37] M. Ablikim *et al.* (BESIII Collaboration), Phys. Rev. D **83**, 112005 (2011).
[38] M. Ablikim *et al.* (BESIII Collaboration), Phys. Rev. D **81**, 052005 (2010).
[39] M. Ablikim *et al.* (BESIII Collaboration), Phys. Rev. D **92**, 112008 (2015).
[40] M. Ablikim *et al.* (BESIII Collaboration), Phys. Rev. Lett. **105**, 261801 (2010).
[41] M. Ablikim *et al.* (BESIII Collaboration), Phys. Rev. D **87**, 012002 (2013).



M. Ablikim,[1] M. N. Achasov,[4,c] P. Adlarson,[77] X. C. Ai,[82] R. Aliberti,[36] A. Amoroso,[76a,76c] Q. An,[73,59,a] Y. Bai,[58] O. Bakina,[37] Y. Ban,[47,h] H.-R. Bao,[65] V. Batozskaya,[1,45] K. Begzsuren,[33] N. Berger,[36] M. Berlowski,[45] M. Bertani,[29a] D. Bettoni,[30a] F. Bianchi,[76a,76c] E. Bianco,[76a,76c] A. Bortone,[76a,76c] I. Boyko,[37] R. A. Briere,[5] A. Brueggemann,[70] H. Cai,[78] M. H. Cai,[39,k,l] X. Cai,[1,59] A. Calcaterra,[29a] G. F. Cao,[1,65] N. Cao,[1,65] S. A. Cetin,[63a] X. Y. Chai,[47,h] J. F. Chang,[1,59] G. R. Che,[44] Y. Z. Che,[1,59,65] C. H. Chen,[9] Chao Chen,[56] G. Chen,[1] H. S. Chen,[1,65] H. Y. Chen,[21] M. L. Chen,[1,59,65] S. J. Chen,[43] S. L. Chen,[46] S. M. Chen,[62] T. Chen,[1,65] X. R. Chen,[32,65] X. T. Chen,[1,65] X. Y. Chen,[12,g] Y. B. Chen,[1,59] Y. Q. Chen,[35] Y. Q. Chen,[16] Z. J. Chen,[26,i] Z. K. Chen,[60] S. K. Choi,[10] X. Chu,[12,g] G. Cibinetto,[30a] F. Cossio,[76c] J. Cottee-Meldrum,[64] J. J. Cui,[51] H. L. Dai,[1,59] J. P. Dai,[80] A. Dbeyssi,[19] R. E. de Boer,[3] D. Dedovich,[37] C. Q. Deng,[74] Z. Y. Deng,[1] A. Denig,[36] I. Denysenko,[37] M. Destefanis,[76a,76c] F. De Mori,[76a,76c] B. Ding,[68,1] X. X. Ding,[47,h] Y. Ding,[35] Y. Ding,[41] Y. X. Ding,[31] J. Dong,[1,59] L. Y. Dong,[1,65] M. Y. Dong,[1,59,65] X. Dong,[78] M. C. Du,[1] S. X. Du,[82] S. X. Du,[12,g] Y. Y. Duan,[56] P. Egorov,[37,b] G. F. Fan,[43] J. J. Fan,[20] Y. H. Fan,[46] J. Fang,[1,59] J. Fang,[60] S. S. Fang,[1,65] W. X. Fang,[1]

Y. Q. Fang,[1,59] R. Farinelli,[30a] L. Fava,[76b,76c] F. Feldbauer,[3] G. Felici,[29a] C. Q. Feng,[73,59] J. H. Feng,[16] L. Feng,[39,k,l] Q. X. Feng,[39,k,l] Y. T. Feng,[73,59] M. Fritsch,[3] C. D. Fu,[1] J. L. Fu,[65] Y. W. Fu,[1,65] H. Gao,[65] X. B. Gao,[42] Y. Gao,[73,59] Y. N. Gao,[47,h] Y. N. Gao,[20] Y. Y. Gao,[31] S. Garbolino,[76c] I. Garzia,[30a,30b] P. T. Ge,[20] Z. W. Ge,[43] C. Geng,[60] E. M. Gersabeck,[69] A. Gilman,[71] K. Goetzen,[13] J. D. Gong,[35] L. Gong,[41] W. X. Gong,[1,59] W. Gradl,[36] S. Gramigna,[30a,30b] M. Greco,[76a,76c] M. H. Gu,[1,59] Y. T. Gu,[15] C. Y. Guan,[1,65] A. Q. Guo,[32] L. B. Guo,[42] M. J. Guo,[51] R. P. Guo,[50] Y. P. Guo,[12,g] A. Guskov,[37,b] J. Gutierrez,[28] K. L. Han,[65] T. T. Han,[1] F. Hanisch,[3] K. D. Hao,[73,59] X. Q. Hao,[20] F. A. Harris,[67] K. K. He,[56] K. L. He,[1,65] F. H. Heinsius,[3] C. H. Heinz,[36] Y. K. Heng,[1,59,65] C. Herold,[61] P. C. Hong,[35] G. Y. Hou,[1,65] X. T. Hou,[1,65] Y. R. Hou,[65] Z. L. Hou,[1] H. M. Hu,[1,65] J. F. Hu,[57,j] Q. P. Hu,[73,59] S. L. Hu,[12,g] T. Hu,[1,59,65] Y. Hu,[1] Z. M. Hu,[60] G. S. Huang,[73,59] K. X. Huang,[60] L. Q. Huang,[32,65] P. Huang,[43] X. T. Huang,[51] Y. P. Huang,[1] Y. S. Huang,[60] T. Hussain,[75] N. Hüsken,[36] N. in der Wiesche,[70] J. Jackson,[28] Q. Ji,[1] Q. P. Ji,[20] W. Ji,[1,65] X. B. Ji,[1,65] X. L. Ji,[1,59] Y. Y. Ji,[51] Z. K. Jia,[73,59] D. Jiang,[1,65] H. B. Jiang,[78] P. C. Jiang,[47,h] S. J. Jiang,[9] T. J. Jiang,[17] X. S. Jiang,[1,59,65] Y. Jiang,[65] J. B. Jiao,[51] J. K. Jiao,[35] Z. Jiao,[24] S. Jin,[43] Y. Jin,[68] M. Q. Jing,[1,65] X. M. Jing,[65] T. Johansson,[77] S. Kabana,[34] N. Kalantar-Nayestanaki,[66] X. L. Kang,[9] X. S. Kang,[41] M. Kavatsyuk,[66] B. C. Ke,[82] V. Khachatryan,[28] A. Khoukaz,[70] R. Kiuchi,[1] O. B. Kolcu,[63a] B. Kopf,[3] M. Kuessner,[3] X. Kui,[1,65] N. Kumar,[27] A. Kupsc,[45,77] W. Kühn,[38] Q. Lan,[74] W. N. Lan,[20] T. T. Lei,[73,59] M. Lellmann,[36] T. Lenz,[36] C. Li,[48] C. Li,[73,59] C. Li,[44] C. H. Li,[40] C. K. Li,[21] D. M. Li,[82] F. Li,[1,59] G. Li,[1] H. B. Li,[1,65] H. J. Li,[20] H. N. Li,[57,j] Hui Li,[44] J. R. Li,[62] J. S. Li,[60] K. Li,[1] K. L. Li,[39,k,l] K. L. Li,[20] L. J. Li,[1,65] Lei Li,[49] M. H. Li,[44] M. R. Li,[1,65] P. L. Li,[65] P. R. Li,[39,k,l] Q. M. Li,[1,65] Q. X. Li,[51] R. Li,[18,32] S. X. Li,[12] T. Li,[51] T. Y. Li,[44] W. D. Li,[1,65] W. G. Li,[1,a] X. Li,[1,65] X. H. Li,[73,59] X. L. Li,[51] X. Y. Li,[1,8] X. Z. Li,[60] Y. Li,[20] Y. G. Li,[47,h] Y. P. Li,[35] Z. J. Li,[60] Z. Y. Li,[80] H. Liang,[73,59] Y. F. Liang,[55] Y. T. Liang,[32,65] G. R. Liao,[14] L. B. Liao,[60] M. H. Liao,[60] Y. P. Liao,[1,65] J. Libby,[27] A. Limphirat,[61] C. C. Lin,[56] D. X. Lin,[32,65] L. Q. Lin,[40] T. Lin,[1] B. J. Liu,[1] B. X. Liu,[78] C. Liu,[35] C. X. Liu,[1] F. Liu,[1] F. H. Liu,[54] Feng Liu,[6] G. M. Liu,[57,j] H. Liu,[39,k,l] H. B. Liu,[15] H. H. Liu,[1] H. M. Liu,[1,65] Huihui Liu,[22] J. B. Liu,[73,59] J. J. Liu,[21] K. Liu,[74] K. Liu,[39,k,l] K. Y. Liu,[41] Ke Liu,[23] L. C. Liu,[44] Lu Liu,[44] M. H. Liu,[12,g] P. L. Liu,[1] Q. Liu,[65] S. B. Liu,[73,59] T. Liu,[12,g] W. K. Liu,[44] W. M. Liu,[73,59] W. T. Liu,[40] X. Liu,[39,k,l] X. Liu,[40] X. K. Liu,[39,k,l] X. Y. Liu,[78] Y. Liu,[82] Y. Liu,[82] Y. Liu,[39,k,l] Y. B. Liu,[44] Z. A. Liu,[1,59,65] Z. D. Liu,[9] Z. Q. Liu,[51] X. C. Lou,[1,59,65] F. X. Lu,[60] H. J. Lu,[24] J. G. Lu,[1,59] X. L. Lu,[16] Y. Lu,[7] Y. H. Lu,[1,65] Y. P. Lu,[1,59] Z. H. Lu,[1,65] C. L. Luo,[42] J. R. Luo,[60] J. S. Luo,[1,65] M. X. Luo,[81] T. Luo,[12,g] X. L. Luo,[1,59] Z. Y. Lv,[23] X. R. Lyu,[65,p] Y. F. Lyu,[44] Y. H. Lyu,[82] F. C. Ma,[41] H. L. Ma,[1] J. L. Ma,[1,65] L. L. Ma,[51] L. R. Ma,[68] Q. M. Ma,[1] R. Q. Ma,[1,65] R. Y. Ma,[20] T. Ma,[73,59] X. T. Ma,[1,65] X. Y. Ma,[1,59] Y. M. Ma,[32] F. E. Maas,[19] I. MacKay,[71] M. Maggiora,[76a,76c] S. Malde,[71] Q. A. Malik,[75] H. X. Mao,[39,k,l] Y. J. Mao,[47,h] Z. P. Mao,[1] S. Marcello,[76a,76c] A. Marshall,[64] F. M. Melendi,[30a,30b] Y. H. Meng,[65] Z. X. Meng,[68] G. Mezzadri,[30a] H. Miao,[1,65] T. J. Min,[43] R. E. Mitchell,[28] X. H. Mo,[1,59,65] B. Moses,[28] N. Yu. Muchnoi,[4,c] J. Muskalla,[36] Y. Nefedov,[37] F. Nerling,[19,e] L. S. Nie,[21] I. B. Nikolaev,[4,c] Z. Ning,[1,59] S. Nisar,[11,m] Q. L. Niu,[39,k,l] W. D. Niu,[12,g] C. Normand,[64] S. L. Olsen,[10,65] Q. Ouyang,[1,59,65] S. Pacetti,[29b,29c] X. Pan,[56] Y. Pan,[58] A. Pathak,[10] Y. P. Pei,[73,59] M. Pelizaeus,[3] H. P. Peng,[73,59] X. J. Peng,[39,k,l] Y. Y. Peng,[39,k,l] K. Peters,[13,e] K. Petridis,[64] J. L. Ping,[42] R. G. Ping,[1,65] S. Plura,[36] V. Prasad,[34] F. Z. Qi,[1] H. R. Qi,[62] M. Qi,[43] S. Qian,[1,59] W. B. Qian,[65] C. F. Qiao,[65] J. H. Qiao,[20] J. J. Qin,[74] J. L. Qin,[56] L. Q. Qin,[14] L. Y. Qin,[73,59] P. B. Qin,[74] X. P. Qin,[12,g] X. S. Qin,[51] Z. H. Qin,[1,59] J. F. Qiu,[1] Z. H. Qu,[74] J. Rademacker,[64] C. F. Redmer,[36] A. Rivetti,[76c] M. Rolo,[76c] G. Rong,[1,65] S. S. Rong,[1,65] F. Rosini,[29b,29c] Ch. Rosner,[19] M. Q. Ruan,[1,59] N. Salone,[45] A. Sarantsev,[37,d] Y. Schelhaas,[36] K. Schoenning,[77] M. Scodeggio,[30a] K. Y. Shan,[12,g] W. Shan,[25] X. Y. Shan,[73,59] Z. J. Shang,[39,k,l] J. F. Shangguan,[17] L. G. Shao,[1,65] M. Shao,[73,59] C. P. Shen,[12,g] H. F. Shen,[1,8] W. H. Shen,[65] X. Y. Shen,[1,65] B. A. Shi,[65] H. Shi,[73,59] J. L. Shi,[12,g] J. Y. Shi,[1] S. Y. Shi,[74] X. Shi,[1,59] H. L. Song,[73,59] J. J. Song,[20] T. Z. Song,[60] W. M. Song,[35] Y. J. Song,[12,g] Y. X. Song,[47,h,n] S. Sosio,[76a,76c] S. Spataro,[76a,76c] F. Stieler,[36] S. S. Su,[41] Y. J. Su,[65] G. B. Sun,[78] G. X. Sun,[1] H. Sun,[65] H. K. Sun,[1] J. F. Sun,[20] K. Sun,[62] L. Sun,[78] S. S. Sun,[1,65] T. Sun,[52,f] Y. C. Sun,[78] Y. H. Sun,[31] Y. J. Sun,[73,59] Y. Z. Sun,[1] Z. Q. Sun,[1,65] Z. T. Sun,[51] C. J. Tang,[55] G. Y. Tang,[1] J. Tang,[60] J. J. Tang,[73,59] L. F. Tang,[40] Y. A. Tang,[78] L. Y. Tao,[74] M. Tat,[71] J. X. Teng,[73,59] J. Y. Tian,[73,59] W. H. Tian,[60] Y. Tian,[32] Z. F. Tian,[78] I. Uman,[63b] B. Wang,[60] B. Wang,[1] Bo Wang,[73,59] C. Wang,[39,k,l] C. Wang,[20] Cong Wang,[23] D. Y. Wang,[47,h] H. J. Wang,[39,k,l] J. J. Wang,[78] K. Wang,[1,59] L. L. Wang,[1] L. W. Wang,[35] M. Wang,[51] M. Wang,[73,59] N. Y. Wang,[65] S. Wang,[12,g] T. Wang,[12,g] T. J. Wang,[44] W. Wang,[74] W. Wang,[60] W. P. Wang,[36,59,73,o] X. Wang,[47,h] X. F. Wang,[39,k,l] X. J. Wang,[40] X. L. Wang,[12,g] X. N. Wang,[1] Y. Wang,[62] Y. D. Wang,[46] Y. F. Wang,[1,59,65] Y. H. Wang,[39,k,l] Y. J. Wang,[73,59] Y. L. Wang,[20] Y. N. Wang,[78] Y. Q. Wang,[1] Yaqian Wang,[18] Yi Wang,[62] Yuan Wang,[18,32] Z. Wang,[1,59] Z. L. Wang,[74] Z. L. Wang,[2] Z. Q. Wang,[12,g] Z. Y. Wang,[1,65] D. H. Wei,[14] H. R. Wei,[44] F. Weidner,[70] S. P. Wen,[1] Y. R. Wen,[40] U. Wiedner,[3] G. Wilkinson,[71] M. Wolke,[77] C. Wu,[40] J. F. Wu,[1,8] L. H. Wu,[1] L. J. Wu,[20] L. J. Wu,[1,65] Lianjie Wu,[20] S. G. Wu,[1,65] S. M. Wu,[65] X. Wu,[12,g] X. H. Wu,[35]

Y. J. Wu,[32] Z. Wu,[1,59] L. Xia,[73,59] X. M. Xian,[40] B. H. Xiang,[1,65] D. Xiao,[39,k,l] G. Y. Xiao,[43] H. Xiao,[74] Y. L. Xiao,[12,g] Z. J. Xiao,[42] C. Xie,[43] K. J. Xie,[1,65] X. H. Xie,[47,h] Y. Xie,[51] Y. G. Xie,[1,59] Y. H. Xie,[6] Z. P. Xie,[73,59] T. Y. Xing,[1,65] C. F. Xu,[1,65] C. J. Xu,[60] G. F. Xu,[1] H. Y. Xu,[2] H. Y. Xu,[68,2] M. Xu,[73,59] Q. J. Xu,[17] Q. N. Xu,[31] T. D. Xu,[74] W. Xu,[1] W. L. Xu,[68] X. P. Xu,[56] Y. Xu,[12,g] Y. Xu,[41] Y. C. Xu,[79] Z. S. Xu,[65] F. Yan,[12,g] H. Y. Yan,[40] L. Yan,[12,g] W. B. Yan,[73,59] W. C. Yan,[82] W. H. Yan,[6] W. P. Yan,[20] X. Q. Yan,[1,65] H. J. Yang,[52,f] H. L. Yang,[35] H. X. Yang,[1] J. H. Yang,[43] R. J. Yang,[20] T. Yang,[1] Y. Yang,[12,g] Y. F. Yang,[44] Y. H. Yang,[43] Y. Q. Yang,[9] Y. X. Yang,[1,65] Y. Z. Yang,[20] M. Ye,[1,59] M. H. Ye,[8] Z. J. Ye,[57,j] Junhao Yin,[44] Z. Y. You,[60] B. X. Yu,[1,59,65] C. X. Yu,[44] G. Yu,[13] J. S. Yu,[26,i] L. Q. Yu,[12,g] M. C. Yu,[41] T. Yu,[74] X. D. Yu,[47,h] Y. C. Yu,[82] C. Z. Yuan,[1,65] H. Yuan,[1,65] J. Yuan,[46] J. Yuan,[35] L. Yuan,[2] S. C. Yuan,[1,65] X. Q. Yuan,[1] Y. Yuan,[1,65] Z. Y. Yuan,[60] C. X. Yue,[40] Ying Yue,[20] A. A. Zafar,[75] S. H. Zeng,[64] X. Zeng,[12,g] Y. Zeng,[26,i] Y. J. Zeng,[60] Y. J. Zeng,[1,65] X. Y. Zhai,[35] Y. H. Zhan,[60] A. Q. Zhang,[1,65] B. L. Zhang,[1,65] B. X. Zhang,[1] D. H. Zhang,[44] G. Y. Zhang,[20] G. Y. Zhang,[1,65] H. Zhang,[82] H. Zhang,[73,59] H. C. Zhang,[1,59,65] H. H. Zhang,[60] H. Q. Zhang,[1,59,65] H. R. Zhang,[73,59] H. Y. Zhang,[1,59] J. Zhang,[82] J. Zhang,[60] J. J. Zhang,[53] J. L. Zhang,[21] J. Q. Zhang,[42] J. S. Zhang,[12,g] J. W. Zhang,[1,59,65] J. X. Zhang,[39,k,l] J. Y. Zhang,[1] J. Z. Zhang,[1,65] Jianyu Zhang,[65] L. M. Zhang,[62] Lei Zhang,[43] N. Zhang,[82] P. Zhang,[1,8] Q. Zhang,[20] Q. Y. Zhang,[35] R. Y. Zhang,[39,k,l] S. H. Zhang,[1,65] Shulei Zhang,[26,i] X. M. Zhang,[1] X. Y. Zhang,[41] X. Y. Zhang,[51] Y. Zhang,[1] Y. Zhang,[74] Y. T. Zhang,[82] Y. H. Zhang,[1,59] Y. M. Zhang,[40] Y. P. Zhang,[73,59] Z. D. Zhang,[1] Z. H. Zhang,[1] Z. L. Zhang,[56] Z. L. Zhang,[35] Z. X. Zhang,[20] Z. Y. Zhang,[44] Z. Y. Zhang,[78] Z. Z. Zhang,[46] Zh. Zh. Zhang,[20] G. Zhao,[1] J. Y. Zhao,[1,65] J. Z. Zhao,[1,59] L. Zhao,[1] L. Zhao,[73,59] M. G. Zhao,[44] N. Zhao,[80] R. P. Zhao,[65] S. J. Zhao,[82] Y. B. Zhao,[1,59] Y. L. Zhao,[56] Y. X. Zhao,[32,65] Z. G. Zhao,[73,59] A. Zhemchugov,[37,b] B. Zheng,[74] B. M. Zheng,[35] J. P. Zheng,[1,59] W. J. Zheng,[1,65] X. R. Zheng,[20] Y. H. Zheng,[65,p] B. Zhong,[42] C. Zhong,[20] H. Zhou,[36,51,o] J. Q. Zhou,[35] J. Y. Zhou,[35] S. Zhou,[6] X. Zhou,[78] X. K. Zhou,[6] X. R. Zhou,[73,59] X. Y. Zhou,[40] Y. X. Zhou,[79] Y. Z. Zhou,[12,g] A. N. Zhu,[65] J. Zhu,[44] K. Zhu,[1] K. J. Zhu,[1,59,65] K. S. Zhu,[12,g] L. Zhu,[35] L. X. Zhu,[65] S. H. Zhu,[72] T. J. Zhu,[12,g] W. D. Zhu,[42] W. D. Zhu,[12,g] W. J. Zhu,[1] W. Z. Zhu,[20] Y. C. Zhu,[73,59] Z. A. Zhu,[1,65] X. Y. Zhuang,[44] J. H. Zou,[1] and J. Zu[73,59]

(BESIII Collaboration)

[1]*Institute of High Energy Physics, Beijing 100049, People's Republic of China*
[2]*Beihang University, Beijing 100191, People's Republic of China*
[3]*Bochum Ruhr-University, D-44780 Bochum, Germany*
[4]*Budker Institute of Nuclear Physics SB RAS (BINP), Novosibirsk 630090, Russia*
[5]*Carnegie Mellon University, Pittsburgh, Pennsylvania 15213, USA*
[6]*Central China Normal University, Wuhan 430079, People's Republic of China*
[7]*Central South University, Changsha 410083, People's Republic of China*
[8]*China Center of Advanced Science and Technology, Beijing 100190, People's Republic of China*
[9]*China University of Geosciences, Wuhan 430074, People's Republic of China*
[10]*Chung-Ang University, Seoul, 06974, Republic of Korea*
[11]*COMSATS University Islamabad, Lahore Campus, Defence Road, Off Raiwind Road, 54000 Lahore, Pakistan*
[12]*Fudan University, Shanghai 200433, People's Republic of China*
[13]*GSI Helmholtzcentre for Heavy Ion Research GmbH, D-64291 Darmstadt, Germany*
[14]*Guangxi Normal University, Guilin 541004, People's Republic of China*
[15]*Guangxi University, Nanning 530004, People's Republic of China*
[16]*Guangxi University of Science and Technology, Liuzhou 545006, People's Republic of China*
[17]*Hangzhou Normal University, Hangzhou 310036, People's Republic of China*
[18]*Hebei University, Baoding 071002, People's Republic of China*
[19]*Helmholtz Institute Mainz, Staudinger Weg 18, D-55099 Mainz, Germany*
[20]*Henan Normal University, Xinxiang 453007, People's Republic of China*
[21]*Henan University, Kaifeng 475004, People's Republic of China*
[22]*Henan University of Science and Technology, Luoyang 471003, People's Republic of China*
[23]*Henan University of Technology, Zhengzhou 450001, People's Republic of China*
[24]*Huangshan College, Huangshan 245000, People's Republic of China*
[25]*Hunan Normal University, Changsha 410081, People's Republic of China*
[26]*Hunan University, Changsha 410082, People's Republic of China*
[27]*Indian Institute of Technology Madras, Chennai 600036, India*
[28]*Indiana University, Bloomington, Indiana 47405, USA*
[29a]*INFN Laboratori Nazionali di Frascati, INFN Laboratori Nazionali di Frascati, I-00044, Frascati, Italy*

[29b]INFN Sezione di Perugia, I-06100, Perugia, Italy
[29c]University of Perugia, I-06100, Perugia, Italy
[30a]INFN Sezione di Ferrara, INFN Sezione di Ferrara, I-44122, Ferrara, Italy
[30b]University of Ferrara, I-44122, Ferrara, Italy
[31]Inner Mongolia University, Hohhot 010021, People's Republic of China
[32]Institute of Modern Physics, Lanzhou 730000, People's Republic of China
[33]Institute of Physics and Technology, Mongolian Academy of Sciences, Peace Avenue 54B, Ulaanbaatar 13330, Mongolia
[34]Instituto de Alta Investigación, Universidad de Tarapacá, Casilla 7D, Arica 1000000, Chile
[35]Jilin University, Changchun 130012, People's Republic of China
[36]Johannes Gutenberg University of Mainz, Johann-Joachim-Becher-Weg 45, D-55099 Mainz, Germany
[37]Joint Institute for Nuclear Research, 141980 Dubna, Moscow region, Russia
[38]Justus-Liebig-Universitaet Giessen, II. Physikalisches Institut, Heinrich-Buff-Ring 16, D-35392 Giessen, Germany
[39]Lanzhou University, Lanzhou 730000, People's Republic of China
[40]Liaoning Normal University, Dalian 116029, People's Republic of China
[41]Liaoning University, Shenyang 110036, People's Republic of China
[42]Nanjing Normal University, Nanjing 210023, People's Republic of China
[43]Nanjing University, Nanjing 210093, People's Republic of China
[44]Nankai University, Tianjin 300071, People's Republic of China
[45]National Centre for Nuclear Research, Warsaw 02-093, Poland
[46]North China Electric Power University, Beijing 102206, People's Republic of China
[47]Peking University, Beijing 100871, People's Republic of China
[48]Qufu Normal University, Qufu 273165, People's Republic of China
[49]Renmin University of China, Beijing 100872, People's Republic of China
[50]Shandong Normal University, Jinan 250014, People's Republic of China
[51]Shandong University, Jinan 250100, People's Republic of China
[52]Shanghai Jiao Tong University, Shanghai 200240, People's Republic of China
[53]Shanxi Normal University, Linfen 041004, People's Republic of China
[54]Shanxi University, Taiyuan 030006, People's Republic of China
[55]Sichuan University, Chengdu 610064, People's Republic of China
[56]Soochow University, Suzhou 215006, People's Republic of China
[57]South China Normal University, Guangzhou 510006, People's Republic of China
[58]Southeast University, Nanjing 211100, People's Republic of China
[59]State Key Laboratory of Particle Detection and Electronics, Beijing 100049, Hefei 230026, People's Republic of China
[60]Sun Yat-Sen University, Guangzhou 510275, People's Republic of China
[61]Suranaree University of Technology, University Avenue 111, Nakhon Ratchasima 30000, Thailand
[62]Tsinghua University, Beijing 100084, People's Republic of China
[63a]Turkish Accelerator Center Particle Factory Group, Istinye University, 34010, Istanbul, Turkey
[63b]Near East University, Nicosia, North Cyprus, 99138, Mersin 10, Turkey
[64]University of Bristol, H H Wills Physics Laboratory, Tyndall Avenue, Bristol, BS8 1TL, UK
[65]University of Chinese Academy of Sciences, Beijing 100049, People's Republic of China
[66]University of Groningen, NL-9747 AA Groningen, The Netherlands
[67]University of Hawaii, Honolulu, Hawaii 96822, USA
[68]University of Jinan, Jinan 250022, People's Republic of China
[69]University of Manchester, Oxford Road, Manchester, M13 9PL, United Kingdom
[70]University of Muenster, Wilhelm-Klemm-Strasse 9, 48149 Muenster, Germany
[71]University of Oxford, Keble Road, Oxford OX13RH, United Kingdom
[72]University of Science and Technology Liaoning, Anshan 114051, People's Republic of China
[73]University of Science and Technology of China, Hefei 230026, People's Republic of China
[74]University of South China, Hengyang 421001, People's Republic of China
[75]University of the Punjab, Lahore-54590, Pakistan
[76a]University of Turin and INFN, University of Turin, I-10125, Turin, Italy
[76b]University of Eastern Piedmont, I-15121, Alessandria, Italy
[76c]INFN, I-10125, Turin, Italy
[77]Uppsala University, Box 516, SE-75120 Uppsala, Sweden
[78]Wuhan University, Wuhan 430072, People's Republic of China
[79]Yantai University, Yantai 264005, People's Republic of China
[80]Yunnan University, Kunming 650500, People's Republic of China

[81]*Zhejiang University, Hangzhou 310027, People's Republic of China*
[82]*Zhengzhou University, Zhengzhou 450001, People's Republic of China*

[a]Deceased.
[b]Also at the Moscow Institute of Physics and Technology, Moscow 141700, Russia.
[c]Also at the Novosibirsk State University, Novosibirsk, 630090, Russia.
[d]Also at the NRC "Kurchatov Institute," PNPI, 188300, Gatchina, Russia.
[e]Also at Goethe University Frankfurt, 60323 Frankfurt am Main, Germany.
[f]Also at Key Laboratory for Particle Physics, Astrophysics and Cosmology, Ministry of Education; Shanghai Key Laboratory for Particle Physics and Cosmology; Institute of Nuclear and Particle Physics, Shanghai 200240, People's Republic of China.
[g]Also at Key Laboratory of Nuclear Physics and Ion-beam Application (MOE) and Institute of Modern Physics, Fudan University, Shanghai 200443, People's Republic of China.
[h]Also at State Key Laboratory of Nuclear Physics and Technology, Peking University, Beijing 100871, People's Republic of China.
[i]Also at School of Physics and Electronics, Hunan University, Changsha 410082, China.
[j]Also at Guangdong Provincial Key Laboratory of Nuclear Science, Institute of Quantum Matter, South China Normal University, Guangzhou 510006, China.
[k]Also at MOE Frontiers Science Center for Rare Isotopes, Lanzhou University, Lanzhou 730000, People's Republic of China.
[l]Also at Lanzhou Center for Theoretical Physics, Lanzhou University, Lanzhou 730000, People's Republic of China.
[m]Also at the Department of Mathematical Sciences, IBA, Karachi 75270, Pakistan.
[n]Also at Ecole Polytechnique Federale de Lausanne (EPFL), CH-1015 Lausanne, Switzerland.
[o]Also at Helmholtz Institute Mainz, Staudinger Weg 18, D-55099 Mainz, Germany.
[p]Also at Hangzhou Institute for Advanced Study, University of Chinese Academy of Sciences, Hangzhou 310024, China.